

NASA Contractor Report 4198

A Numerical Method for Computing Unsteady 2-D Boundary Layer Flows

Andreas Krainer

PURCHASE ORDER C-80017-F
DECEMBER 1988

(NASA-CR-4198) A NUMERICAL METHOD FOR
COMPUTING UNSTEADY 2-D BOUNDARY LAYER FLOWS
NASA Contractor Report (Naval
Postgraduate School) 62 p

CSCI 200

H1/34

N89-12833

Unclas

0174983



NASA Contractor Report 4198

A Numerical Method for Computing Unsteady 2-D Boundary Layer Flows

Andreas Krainer
Naval Postgraduate School
Monterey, California

Prepared for
Lewis Research Center
under Purchase Order C-80017-F



National Aeronautics
and Space Administration

Scientific and Technical
Information Division

1988

Abstract

A numerical method for calculating unsteady two-dimensional boundary layers in incompressible laminar and turbulent flows is described, and applied to a single airfoil changing its incidence angle in time. The solution procedure adopts a first order panel method with a simple wake model to solve for the inviscid part of the flow, and an implicit finite difference method for the viscous part of the flow. Both procedures integrate in time in a step-by-step fashion, in course of which each step involves the solution of the elliptic Laplace equation and the solution of the parabolic boundary layer equations. The Reynolds shear stress term of the boundary layer equations is modeled by an algebraic eddy viscosity closure, which essentially is the steady Cebeci-Smith model. The location of transition is predicted by an empirical data correlation originating from Michel. Since transition and turbulence modeling are key factors in the prediction of viscous flows, their accuracy will be of dominant influence to the overall results.

The presented methodology offers a decisive cost advantage as compared to solvers of the full Navier-Stokes equations. The efficiency of our method derives from its viscous and inviscid components, which both bypass the far more expensive field solution. Conceptually the method makes no assumptions as to the type of motion or the shape of the airfoil, and is subject only to the limitations imposed by the boundary layer approximation and by the assumption of an irrotational inviscid flow field. As a consequence of the currently employed boundary layer approach, in which the pressure is prescribed, the method cannot cope with the problem of flow separation. Future work is planned to address the problem of unsteady flow separation, which will require an interactive coupling of the inviscid and viscous flow solvers.

PRECEDING PAGE BLANK NOT FILMED

Table of Contents

1. Introduction	1
2. The unsteady potential flow method	5
3. The unsteady boundary layer method	12
Introduction	12
The differential equations, the boundary and initial conditions	13
Signal propagation in unsteady boundary layers	14
The numerical procedure	16
Turbulence modeling and transition	19
Unsteady separation and singularities	21
4. Results and discussion	23
5. Concluding remarks	27
Acknowledgments	28
6. List of references	29
Appendix A. The regular box scheme	32
Appendix B. The characteristic box scheme	35
Appendix C. The upstream boundary conditions	37
Appendix D. Guesses for the initial Newton iteration	40
Appendix E. On instabilities of the near-wall solutions	41

PRECEDING PAGE BLANK NOT FILMED

1. Introduction

The prediction of unsteady viscous flow phenomena is of importance for a variety of aerodynamic devices, including turbomachinery bladings, helicopter rotor blades, wind energy devices, and rapidly maneuvering aircraft. The unsteadiness of the problem can result either from an unsteady onset flow acting on a stationary body, or from an unsteadily moving body in an initially uniform onset flow. Examples for the first type of problems are the flow through the stator of a turbomachine being exposed to the wakes of the previous stages and the flow past aircraft travelling through atmospheric gusts. Examples for the latter type are the flows past rapidly maneuvering aircraft in quiet air and the flow through the vibrating blades of a turbomachine. Many problems of practical interest involve both forms of unsteadiness, like the flowfield surrounding a helicopter rotor, whose blades change both speed and incidence angle and are exposed to the wakes of the previous blades. Most of today's numerical tools hardly can keep up with the complexity of these flows. The majority of today's design methods either assumes inviscid flow conditions or relies upon empirical data correlations. However, the advances in computer technology have initiated the development of methods, which do take account of viscous effects. Large efforts are now under way in order to attempt the solution of the full Navier-Stokes equations or of some asymptotic approximation to the Navier-Stokes equations.

Although the full Navier-Stokes equations are generally accepted as the exact physical model of the flow, asymptotic approximations continue to be pursued because of their relative merits with regard to computer time and storage and because of their ability of promoting the understanding of flows. Of course, asymptotic approximations cannot be expected to be universally applicable and their inadequate use can lead to numerical breakdowns. The Goldstein singularity /22/ in steady boundary layers and Van Dommelen's singularity /43/ in unsteady boundary layers are prominent examples of this very fact. Yet the appearance of singularities can be considered to be an advantage, since they often reveal the transition to another flow regime and indicate the need for another asymptotic description. Under a disadvantageous scenario the solution of an asymptotic approximation might simply diverge from the Navier-Stokes solution without giving any indication. In spite of the inherent limitations of approximations it is the simplified model that allows us to gain fundamental knowledge by reducing the problem to its essential.

The Navier-Stokes equations are of the elliptic type, which means that information propagates in all directions. In principle, information is transmitted via pressure, via the viscous (and turbulent) stress gradients, and via the local velocity. While the signals of the first two types spread in all directions, the signals of the third are convected with the stream. A solution of the full Navier-Stokes equations requires thus a simultaneous processing of the pressure, the velocity components, and the stress tensor throughout the flowfield, which for the present rules out this procedure as an engineering tool because of costs. Simplifications of the Navier-Stokes equations consist of restricting the signal propagation in certain parts of the flowfield. Provided that the longitudinal stress gradients are small compared to the cross-stream shear gradients, the signals due to the viscous stresses can be assumed to not propagate in the streamwise direction. In practice, this is achieved by omitting these minor stress terms, which leads to the so-called parabolized or thin-layer Navier-Stokes equations. The first name refers to the partially changed characteristics of the new equations, although the elliptic behavior is retained due to the pressure signals being sent in all directions. The second name indicates that the viscous effects ought to be confined to a wall-bounded region, whose cross-stream dimension is small. In contrast to the boundary layer equations this approach retains the momentum equation across the viscous layer, so that the strong

coupling between inner viscous and outer inviscid flow is maintained. The classical boundary layer approximation goes one step further: In addition to limiting the viscous effects to a thin layer, the calculation of the pressure is separated from the calculation of the viscous flowfield. This leaves one flowfield, in which there are no signals due to viscous stress gradients, and another one, in which there are no pressure signals. The flowfield that determines the pressure can be described by the Euler equations, which evolve from the Navier-Stokes equations by omitting all viscous terms. The viscous layer is governed by Prandtl's boundary layer equations, in which longitudinal diffusion terms have been dropped and which require the pressure being imposed from outside. This simplest set of equations can be developed under the assumption that inside the boundary layer the gradient of any velocity component in the cross-stream direction is much larger than its gradient in the streamwise direction. It is this very condition, which makes the classical boundary layer equations so effective and at the same time so vulnerable. Because the solution of the boundary layer equations can be obtained by progressing step by step in the streamwise direction (a consequence of the parabolic characteristics), boundary layers are by an order of magnitude less costly to solve than viscous flowfields governed by the Navier-Stokes equations. Because the outer flowfield has been decoupled from the viscous layer (a consequence of the dropped momentum equation in the cross-stream direction and of the imposed pressure on the boundary layer), the boundary layer approach does not apply in situations where the viscous layer has a substantial effect on the outer inviscid flowfield. This prevents regions of separated flow from successful treatment by means of the classical boundary layer theory.

Since the appearance of the boundary layer theory in 1904, many attempts have been undertaken to turn the boundary layer approach into an even more versatile tool and to remove some of its limitations. It was found that the Goldstein singularity, which occurs at the point of zero wall shear in steady boundary layers subject to a prescribed pressure distribution, can be removed by prescribing instead the displacement thickness (or the wall shear /5/). While in direct methods the pressure is determined by the inviscid flow and the displacement thickness by the viscous flow, such a boundary condition would swap the roles of pressure and displacement thickness. Thus inverse methods determine the velocity at the boundary layer edge, and consequently the pressure along the boundary layer, as part of the viscous flow solution. But inverse methods introduced new problems (slow convergence), and also common sense suggests that the flow over an airfoil involves both types of interaction. This led to the development of the interactive boundary layer methods, which are designed to ensure interaction in both ways, that is the viscous flow is allowed to influence the inviscid flow and vice versa. The essence of these methods is an interactive boundary condition, which prescribes at the boundary layer edge a linear combination of the unknown velocity and displacement thickness. The overall solution is now obtained in an iterative process, which accounts for the displacement effect upon the outer inviscid flow. So far, interactive boundary layer procedures have an outstanding record in dealing with such diversified problems like subsonic and transonic flows /29/, single airfoil /10/, multi-element airfoil and airfoil-spoiler flows /29/, steady /45/ and unsteady flows /20,23/. Interactive boundary layer procedures can be considered as inexpensive alternatives to the Navier-Stokes solvers, since they are, as well, capable of handling (moderately) separated flows.

Concepts similar to those of the steady boundary layer can be applied to the unsteady problem. Unfortunately, our knowledge of unsteady boundary layers is less sound and the status of unsteady procedures is less settled than that of steady ones. For example, the criterion of unsteady flow separation is still a matter of discussion. While in steady boundary layers the point of separation coincides with the point of zero wall shear, such a simple

correlation does not exist for unsteady boundary layers. There have been other separation criteria proposed (for a review see /41/ or /47/), like the Moore-Rott-Sears criterion, which derives from a boundary layer along a moving wall, but their universal applicability remains disputed. It is, however, clear that the point of zero wall shear, in general, will be nonsingular in unsteady boundary layers, and consequently direct methods do not experience a Goldstein-like singularity at this very point. But unsteady boundary layers are by no means free of singularities: With the external velocity as prescribed datum the unsteady boundary layer of an impulsively started cylinder develops the so-called Van Dommelen singularity (which is not of the Goldstein type) within a finite time. Since the discovery of this singularity (in 1977) numerous attempts have been made to remove this singularity, but none of them could achieve more than to delay its appearance. Certainly, the development of unsteady interactive boundary layer procedures is only at its beginning, and further work is needed in order to better understand unsteady flow separation.

As yet another problem of great importance, concerning both Navier-Stokes methods and boundary layer methods alike, has not been solved in a satisfactory way. Both Navier-Stokes equations and asymptotic approximations do not contain enough information about turbulence to form a closed set of equations. The unknown Reynolds stresses must be modeled empirically, so that the number of unknowns is reduced to equal the number of equations. The most common approach is to define an eddy viscosity, which may be obtained from the solution of either algebraic equations or differential equations, like the transport equation of turbulence energy. Algebraic models offer simplicity and accuracy over the range of data upon which they are based, while transport models are usually applicable to a wider range of flows, such as flows with a strong adverse pressure gradient and extensively separated flows. But not only the modeling of turbulence, also the prediction of transition holds plenty of uncertainties. Since flows past airfoils, in particular at low Reynolds numbers, comprise laminar, transitional, and turbulent regimes, there is the need to specify both the onset of transition and the extent of the region between laminar and turbulent flow. The choice lies here between empirical data correlations, which relate the locus of transition to some mean flow parameter, and linear stability theory, which requires the solution of the linear stability equations and subsequently correlates the onset of transition to the amplification ratio of disturbances. From a practical point of view the former methods are advantageous because of the ease of numerical implementation, while the latter ones offer a greater degree of generality. Since both transition and turbulence have a dominant effect on the flow results, their importance hardly can be overestimated and their underlying assumptions cannot be scrutinized enough. A further approximation of all engineering methods requires that the time-accurate equations are always replaced by time-averaged equations. For the time being the solution of the full Navier-Stokes equations with a time-scale that would resolve the motion of turbulent eddies is simply not feasible with a reasonable employment of computer resources. Therefore the Navier-Stokes equations and all the asymptotic approximations are time-averaged over a time-scale that is too large to resolve any scales of the motion in turbulent flow, yet is small compared to the aerodynamic time-scale of the unsteady flow itself. So if we, earlier in this chapter, referred to procedures to solve the Navier-Stokes equations or some reduced form of them, we implicitly meant the solution of the Reynolds-averaged equations, which do not resolve turbulence.

Finally, we want to focus the discussion on the approach pursued here. The subject, we examine, is the unsteady two-dimensional flow of an incompressible viscous fluid past a single airfoil. The fluid is assumed to be initially at rest or in uniform motion and the unsteadiness of the flow shall result solely from the unsteadily moving airfoil. There are no assumptions made as to the type of motion the airfoil is executing or as to the shape of the

airfoil. The chosen methodology attempts the solution of the complete flow by a synthesis of an outer potential flow and an inner boundary layer flow. The solution of the outer inviscid flowfield is obtained by an unsteady panel method, which, in contrast to steady methods, has to model the continuous shedding of vorticity into the trailing wake. As in the original panel method by Smith and Hess /24/, the singularity distribution is made up by uniform source panels and a uniform vorticity around the airfoil. In addition, the wake consists of a vorticity panel, which is attached to the trailing edge, and a series of point vortices, which are convected downstream with the local particle speed. The solution of the viscous flow is determined by a finite difference approximation to the boundary layer equations cast in dimensionless, physically transformed variables. In order to properly account for flow reversals, which in unsteady flows are not necessarily related to flow separations, the currently employed method utilizes a numerical technique advocated by Cebeci, that is the use of both the regular box scheme /9/ and the characteristic box scheme /7,12,13/. In addition, the solution of the unsteady boundary layer equations requires that initial and upstream boundary conditions be provided. On the assumption that the time derivatives of all variables vanish at the initial time (of the computational domain), the initial conditions can be obtained from a steady-state solution. The upstream boundary conditions are generated by a procedure, involving the iterative use of the characteristic box scheme, which allows for both the movement of the stagnation point and the eventual occurrence of flow reversals. The Reynolds shear stress term is approximated by means of the eddy viscosity concept, using the algebraic formulation of the Cebeci-Smith model /6/. The onset of transition is predicted by an empirical data correlation originating from Michel /33/, while the finite region of transition is taken into account by an intermittency distribution stemming from Chen and Thyson /14/. As of now the method performs calculations in the direct mode only, that is the outer boundary condition prescribes the external velocity, which prevents the method from successfully dealing with separated flows. The interactive coupling of the potential flow and the boundary layer flow, which shall permit the inclusion of separated flow regions, is going to be addressed in the near future.

The present report is divided into five chapters, the first of which is this introduction. The second chapter is concerned with the formulation of the unsteady panel method, in particular, attention is given to the unsteady pressure equation, the unsteady Kutta condition, and the wake model. The third chapter is devoted to the description of the unsteady boundary layer method. In order to gain a better understanding of the numerical necessities, first the mechanism of signal propagation in unsteady boundary layers is outlined. Subsequently, the finite difference approximation to the unsteady boundary layer equations is introduced, and the algorithms of the numerical solution are discussed briefly. A rather short account is then given of the modeling of turbulence and of the prediction of transition. A preliminary reflection on unsteady flow separation concludes the third chapter. The results of the flow past a single airfoil undergoing a ramp-change in angle of attack are presented in the fourth chapter. The final and fifth chapter identifies summary conclusions and addresses some of the goals of future work. The reader is alerted to the fact that the present report is of an interim nature covering the period from September 1986 through August 1987.

2. The unsteady potential flow method

The calculation of the inviscid incompressible flow over an airfoil, which is undergoing an arbitrary time-dependent motion, is performed by a panel method that includes a model for the continuous shedding of vorticity into the trailing wake. The existence of a vortex sheet behind the airfoil can be explained by the Helmholtz theorem, which requires that any change in the circulation around the airfoil must be matched by the appearance of an equal countervortex somewhere in the flowfield. Naturally, the appearance of this countervortex takes place at the trailing edge of the airfoil. Since free vortices move with the particles of the surrounding fluid, all countervortices together will form a sheet, which extends from the trailing edge in the downstream direction. Also the bound vortex of an airfoil in steady flow is balanced by a series of countervortices, which has been generated when the airfoil started its motion. But there the existence of these countervortices does not present any difficulties, because the countervortices had been carried too far downstream to have any effect on the flow at the airfoil. Not so in an unsteady flow, in which the airfoil may experience a continuous change of circulation: The countervortices will stay for some time close enough to affect the flow over the airfoil, though their influence will lessen as they travel downstream. The flow over the airfoil in turn will influence the process of vortex shedding and the shape of the vortex sheet in the near wake, while the flow in the far wake is determined mainly by the vorticity which is stored up there. The presence of the countervortices provides the flow with kind of a memory in that the flow at a particular time is affected by the bound circulation of the past. Any mathematical model that describes unsteady flows must hence be equipped with a mechanism to simulate the process of shedding vorticity into the wake, which distinguishes the unsteady flow from its steady counterpart.

The inviscid flow solution is based on four principles, namely the conservation of mass, the conservation of momentum, the conservation of vorticity, and the condition of irrotational flow. The basic governing equation, comprising the continuity equation of an incompressible fluid ($\text{div } \vec{V} = 0$) and the condition of irrotational flow ($\text{curl } \vec{V} = 0$), is the Laplace equation

$$\text{div}(\text{grad } \phi) = 0 \quad (2.1)$$

with $\phi(X, Y, t)$ denoting the potential for the velocity. Irrotationality is the necessary and sufficient condition for the existence of a velocity potential such that $\vec{V} = \text{grad } \phi$. Interestingly, the Laplace equation applies to steady and unsteady flows alike, because of which unsteady flow methods can be obtained by extending steady flow models. Another significant feature of the Laplace equation is that the velocity turns out to be decoupled from the pressure and hence the calculation of velocity and pressure can be performed separately and consecutively. Following the calculation of the velocity flowfield, the pressure can be determined from the Bernoulli equation, which derives from the law of conservation of momentum under the previously stated assumptions

$$\frac{p - p_\infty}{\rho} + \frac{V^2}{2} + \frac{\partial \phi}{\partial t} = 0 \quad (2.2)$$

This form of the Bernoulli equation refers to an inertial frame of reference $[X, Y]$, in which the motion of the fluid is described by the velocity $V(X, Y, t)$. Since it is more convenient to pose the problem in a frame of reference that is attached to the moving airfoil, the Bernoulli equation must be written for a moving frame of reference. With $\vec{V}_S(x, y, t)$ denoting the velocity of a point in the moving system $[x, y]$ with respect to the inertial system, the ve-

locity $\vec{v}(x, y, t)$ of a fluid particle as viewed in the moving frame can be related to the velocity $\vec{V}(x, y, t)$ of the same fluid particle as viewed in the inertial frame according to

$$\vec{V} = \vec{V}_S + \vec{v} = \vec{V}_A + \Omega(x\vec{j} - y\vec{i}) + \vec{v} \quad (2.3)$$

The velocity $\vec{V}_S(x, y, t)$ can further be decomposed into a translational speed, $\vec{V}_A(t)$, and a rotational speed, $\Omega(t)$. In the following it will be assumed that the translational speed V_A includes the free stream U_∞ , so that the fluid particles are initially at rest with respect to the inertial system. As the airfoil approaches a particular station in the inertial system, an observer there could perceive the initially motionless fluid particles making way for the airfoil. Although the fluid particles might neither return to their original position nor become stationary within a finite time, they do not leave their original neighborhood. Because fluid particles (as viewed in the inertial system) do only get disturbed from their original position, V and ϕ will be called the disturbance velocity and the disturbance potential, respectively. But while the velocity can be given with respect to any frame of reference, this is not the case for the potential. Vorticity and circulation are, as well as the velocity, concepts relative to a frame of reference, and therefore the same flow, viewed from different frames, may well be either irrotational or rotational. This, in general, will not allow to introduce a velocity potential for the flowfield as seen in the moving system. But we have the option to write the velocity potential in terms of other independent variables. So if we replace the disturbance potential $\phi(X, Y, t)$ by the disturbance potential $\phi(x, y, t)$, which describes the very same flowfield ($\vec{V} = \text{grad } \phi$), we arrive at the Bernoulli equation for the moving frame

$$\frac{p - p_\infty}{\rho} - \frac{V_S^2}{2} + \frac{v^2}{2} + \frac{\partial \phi}{\partial t} = 0 \quad (2.4)$$

The Laplace equation and the Bernoulli equation (with a zero time-derivative of the potential) would be sufficient to determine steady flow. Unsteady flow calls for one additional principle, the conservation of vorticity. The Helmholtz theorem requires that the total circulation in a potential flowfield must be preserved, which, interpreted for an airfoil flow, means that the change in circulation around the airfoil must be matched by an equal and opposite change of vorticity in the wake.

Next we consider the boundary conditions, which complement the governing equations in order to form a solvable problem. There are two of them, namely the condition of tangential flow and the Kutta condition. The condition of tangential flow is easily stated in terms of the moving frame of reference, that is the velocity \vec{v} of a fluid particle with respect to the airfoil (moving frame of reference) must not have a component normal to the surface of the airfoil

$$\vec{v} \cdot \vec{n} = 0 \quad (2.5)$$

In addition, another boundary condition is needed to uniquely establish a solution. It is common practice to make use of the empirical Kutta condition for that purpose. The Kutta condition postulates zero load at the trailing edge in order to ensure that the flows of upper and lower surface leave the airfoil smoothly. The trouble with this procedure is that an inviscid flow method makes use of a condition that derives from an experimental observation in a viscous fluid. It is thus the consideration of viscosity, which allows to fix the circulation around the airfoil and consequently yields a unique solution of the inviscid flow problem. While in steady flows the use of the Kutta condition is well accepted, there is experimental evidence that the condition of zero load at the trailing edge is violated in certain

unsteady flows. But in the absence of anything better, most - if not all - unsteady methods (including the present approach) stick to the zero load trailing edge condition. In general such a condition will not lead to a stagnation point at the trailing edge, nor to velocities of equal magnitude on upper and lower surface at the trailing edge. Only when the rate of change in circulation is zero, that is steady flow conditions, will the velocities approach the same value. But this is, on physical grounds, more acceptable than having a nonzero pressure differential at the trailing edge, and furthermore the zero load condition does not conflict with the shedding of vorticity at the trailing edge.

We will now turn to the numerical technique to solve the unsteady potential flow. Because the principle of superposition applies to the linear Laplace equation, the flowfield can be built up by simple elementary flows. The significance of elementary solutions lies in that they automatically satisfy the Laplace equation and the task left is to compose them such that they also satisfy the boundary conditions. For obvious reasons numerical techniques seek to utilize the simplest elementary flows available, which are those of a point source, a point sink, and a point vortex. There are many legitimate choices of these elementary solutions (also termed singularities), and there are a great many ways to distribute them, preferably, however, on or close to the surface of the airfoil. Correspondingly, numerous techniques are now available to achieve the numerical solution of an inviscid incompressible flow. The most popular technique is associated with Smith and Hess /24/, who devised the so-called panel method in the early sixties. The first extension of the panel method to the unsteady problem was given by Giesing in 1968 /21/, and since then a couple of authors, amongst them Basu and Hancock /2/, and more recently Kim and Mook /27/, followed proposing some variations of the unsteady approach. With the exception of the wake, which needs to be simulated in the unsteady flow model, steady and unsteady techniques are virtually identical. In order to solve the unsteady problem, the flow is calculated at successive intervals of time by exercising the steady procedure step by step in time, starting from some initial airfoil position and proceeding along the airfoil flight path. The representation of the wake can be as simple as a series of point vortices spread along a straight line, or as sophisticated as continuously distributed vorticity along a curved sheet, whose shape is the result of the convection of fluid particles being attached to it. At each time interval the airfoil supplies the wake with some more vorticity (provided the circulation around the airfoil is changing), and the already existing vorticity moves correspondingly downstream. Only this mechanism is essential for the successful outcome of any technique, while the choice of singularities, the use of higher order panels and singularity distributions, as well as the sophistication of the wake model are of secondary importance.

Regarding the numerical approach, in particular how the airfoil is represented geometrically and which type of singularity distributions is used, the present approach follows closely the original panel method of Smith and Hess /24/, while with regard to the modeling of the wake, the present approach adopts the procedure as advocated by Basu and Hancock /2/. In detail: The airfoil surface is divided into N planar elements, termed panels, such that the airfoil contour is approximated by an inscribed polygon. The first element (index 1) starts on the lower surface at the trailing edge, then elements proceed clockwise around the airfoil contour, until the last element (index N) reaches again the trailing edge. A uniform source distribution and a uniform vorticity distribution is placed on each panel, whereby the source strength $(\sigma_j)_k$ varies from element to element, while the vortex strength γ_k is the same for all elements at a given instant of time. The wake consists of a single vorticity panel attached as an additional element to the trailing edge, through which the vorticity is shed into the wake, and a series of discrete point vortices which are carried downstream with the particles of the surrounding fluid. A uniform vorticity distribution of strength $(\gamma_w)_k$ is placed on the wake panel, which is further characterized by its length Δ_k and its inclination Θ_k with re-

spect to the x-axis of the airfoil frame. After each time step the vorticity of the wake panel is assumed to be concentrated into a single point vortex, which detaches from the airfoil and starts moving with the stream. At the same time one wake element detaches from the airfoil, a new one is created. The downstream wake of point vortices is thus formed by the shed vorticity of previous timesteps.

The following considerations assume that the calculation of $(k-1)$ timesteps has been completed and refer consequently to the solution of the k th timestep. At each timestep the location of all singularities is frozen and hence any relative motion between singularities is not accounted for. The boundary condition of tangential flow is imposed at collocation points, which are taken as the exterior midpoints of the elements. Using the concept of influence coefficients the tangential flow condition of the i th element can be written according to

$$\sum_{j=1}^N A_{ij}^n (\sigma_j)_k + \gamma_k \sum_{j=1}^N B_{ij}^n + (B_{i,N+1}^n)_k (\gamma_w)_k + \sum_{m=1}^{k-1} (C_{im}^n)_k (\Gamma_{m-1} - \Gamma_m) = [\vec{V}_A + \Omega(x^j - y^i)]_k \cdot [\vec{n}_i]_k \quad (2.7)$$

This condition equilibrates the normal velocity of a fluid particle, that an observer at the midpoint of the i th element would notice in undisturbed flow (right hand side), and the normal velocity at the very same place due to the perturbation of the flow (left hand side). The following singularities are assumed to contribute to the flow perturbation: the source (first term) and vorticity distributions (second term) on the airfoil contour, the vorticity distribution of the wake panel (third term), and the discrete point vortices in the wake (fourth term). The coefficients A , B , and C represent the effect from one panel (point vortex) to another panel, because of which they are called influence coefficients. More precisely, they are defined as the velocity induced by the singularity distribution of a single element (or by a single point vortex) of unit strength. The first subscript of an influence coefficient identifies here the location where the velocity is induced, the second subscript denotes the element (or the point vortex) which is causing the very velocity, and the superscript indicates which component of the induced velocity is given by the denoted coefficient. The above introduced influence coefficients mean thus the following:

- A_{ij}^n represents the normal velocity component at the midpoint of the i th element due to a source distribution of unit strength on the j th element.
- B_{ij}^n represents the normal velocity component at the midpoint of the i th element due to a vorticity distribution of unit strength on the j th element.
- C_{im}^n represents the normal velocity component at the midpoint of the i th element due to the m th point vortex of unit strength.

The auxiliary boundary condition, which is supposed to uniquely establish the flow solution, is taken as the Kutta condition of zero load at the trailing edge ($p_{upper} = p_{lower}$). The Kutta condition is satisfied in an approximate fashion in that the pressures of upper and lower surface are equated at the midpoints of the elements adjacent to the trailing edge (first and last panel). Relating the rate of change of the difference in the velocity potentials of upper and lower surface at the trailing edge with the rate of change in the circulation around the airfoil, the Kutta condition can be expressed in terms of the vorticity strengths of the current and the previous timestep

$$[(v_1^t)_k]^2 - [(v_N^t)_k]^2 = 2 \left[\frac{\partial(\phi_n - \phi_1)}{\partial t} \right]_k = 2 \left[\frac{\partial \Gamma}{\partial t} \right]_k = 2l \frac{\gamma_k - \gamma_{k-1}}{t_k - t_{k-1}} \quad (2.8)$$

where Γ denotes the circulation around the airfoil and l is the airfoil perimeter. The time-derivative of the circulation is here approximated by a first-order accurate backward finite difference.

In contrast to the steady flow solution there is one additional condition to be imposed on unsteady flows. The Helmholtz theorem postulates that any change in the circulation around the airfoil must be matched by a change of vorticity in the wake of equal magnitude and opposite sign. If this postulate is evaluated in terms of our wake model, the following relationship is obtained

$$\Delta_k (\gamma_w)_k = l (\gamma_{k-1} - \gamma_k) \quad (2.9)$$

This equation states that the vorticity in the wake element be equal to the negative change of circulation around the airfoil with respect to the previous timeline. This equation is further based on the assumption that the circulation around the free point vortices in the downstream wake does not change after the point vortex is formed from the spread vorticity along the wake panel.

Before we continue with the actual algorithm, we summarize briefly the setup. The following unknowns have been introduced in the equations (2.7) through (2.9): There are the N unknown source strengths $(\sigma_s)_k$ and the one unknown vorticity strength γ_k along the elements on the airfoil, and there are the unknown vorticity strength $(\gamma_w)_k$, length Δ_k , and orientation Θ_k of the wake panel. The last two of which did not show up in the equations, but they have to be known as part of the geometrical setup in order to calculate the influence coefficients due to the wake panel. This makes a total of $N + 4$ unknowns, which must be matched by an equal number of equations. So far the following equations have been identified:

1. The flow tangency conditions represent a system of N equations.
2. The Kutta condition is a single equation that determines the circulation around the airfoil.
3. The Helmholtz theorem is another single equation that provides a relation for the strength of the vorticity distribution along the wake element.

Clearly we are short of two equations, which ought to address the length and orientation of the wake element. Following a suggestion by Basu and Hancock, the following assumptions are made about the geometry of the wake panel:

1. The wake panel is oriented in the direction of the local resultant velocity at its midpoint

$$\tan \Theta_k = \frac{(v_w^y)_k}{(v_w^x)_k} \quad (2.10)$$

with $(v_w^x)_k$ and $(v_w^y)_k$ denoting the x- and y-velocity components at the midpoint of the wake panel, as viewed in the (moving) airfoil frame of reference.

2. The length of the wake panel is proportional to the magnitude of the local resultant velocity at its midpoint and to the timestep

$$\Delta_k = \sqrt{[(v_w^x)_k]^2 + [(v_w^y)_k]^2} (t_k - t_{k-1}) \quad (2.11)$$

whereas the velocity components $(v_w^x)_k$ and $(v_w^y)_k$ (in both equations (2.10) and (2.11)) do not include the effect of the wake element on itself.

Although the majority of the equations is linear, the nonlinearities in the Kutta condition and in the two equations for Δ_k and Θ_k necessitate an iterative solution procedure. How-

ever, the effect of the nonlinearly involved variables (Δ_k and Θ_k) is weak enough to allow for a linear algorithm being applied to the system of flow tangency conditions, in which the nonlinear variables are treated as known quantities given by the previous cycle of iteration. Each cycle closes by recomputing improved values for the nonlinear variables. Thus the overall solution is obtained in successive approximations, which involve the following steps:

1. Before the calculation of a new timeline can get started, the length and the orientation of the wake element must be guessed, for example from the previous timeline.
2. Making use of the Helmholtz theorem (the vorticity strength of the wake element is replaced by an expression of the unknown γ_k and the known γ_{k-1}) the system of flow tangency conditions can be rearranged in form of the following matrix equation

$$[A] \{\sigma\}_k = \gamma_k \{B\}_k + \{C\}_k \quad (2.12)$$

where $[A]$ is a $N \times N$ matrix, $\{B\}_k$ and $\{C\}_k$ are N -dimensional vectors, respectively. This matrix equation represents a linear system for the unknown source strengths $(\sigma_j)_k$ in terms of the yet undetermined vorticity strength γ_k .

3. With these results the Kutta condition turns into a quadratic equation for the unknown vorticity strength γ_k .
4. Under the assumption of an accurately determined wake element steps 2 and 3 establish a unique solution of the flow. Now the length and the orientation of the wake panel are recomputed and the procedure proceeds with step 2 if Δ_k and Θ_k have not converged to a desired accuracy.
5. In case of convergence the calculation of the k th timeline is completed by determining the velocity and pressure distributions on the airfoil.

Due to the minor effect of an inaccurately assumed wake panel on the overall flow results, the procedure converges extremely fast, say within two and four iterations. The numerical procedure can further be accelerated by taking account of the fact that the matrix $[A]$ does not change with the iterations nor with time. Hence the most time consuming numerical step, which is the LU-decomposition of the matrix $[A]$, needs to be exercised only once. However, a record of the manipulations performed on the right hand side during the initial timestep must be kept in order to repeat these manipulations on the right hand sides of the following iterations and timelines.

Once the source strengths and circulation around the airfoil have been determined, one can proceed with the computation of the velocities throughout the flowfield. Utilizing again the concept of influence coefficients the tangential velocities at the midpoint of the i th element can be expressed in the following form

$$(V_i^t)_k = \sum_{j=1}^N A_{ij}^t (\sigma_j)_k + \gamma_k \sum_{j=1}^N B_{ij}^t + (B_{i,N+1}^t)_k (\gamma_w)_k + \sum_{m=1}^{k-1} (C_{im}^t)_k (\Gamma_{m-1} - \Gamma_m) \quad (2.13)$$

$$(v_i)_k = (v_i^t)_k = (V_i^t)_k - [\vec{V}_A + \Omega (x_i \vec{j} - y_i \vec{i})]_k \cdot [\vec{t}_i]_k \quad (2.14)$$

$(V_i^t)_k$ in equation (2.13) refers here to the tangential velocity as viewed in the inertial frame of reference, whereas $(v_i^t)_k$ in equation (2.14) refers to the tangential velocity as viewed in the moving frame of reference. If there is interest in the load on the airfoil, then the unsteady Bernoulli equation must be resolved with respect to the pressure to provide this kind of information. The pressure coefficient in an unsteady flow is given by

$$C_p = -\frac{2}{U_\infty^2} \frac{\partial \phi}{\partial t} + \frac{V_s^2}{U_\infty^2} - \frac{v^2}{U_\infty^2} \quad (2.15)$$

In contrast to the steady flow, the unsteady pressure coefficient includes a contribution due to the rate of change of the velocity potential. Since the value of $\partial\phi/\partial t$ will be approximated by a first-order accurate backward finite difference, the velocity potential must be evaluated at each timeline. The calculation of the velocity potential is accomplished by an integration of the velocity flowfield along a line extending from a position, which is sufficiently far upstream so that disturbance effects there are negligibly small, to the point of interest. In particular, the integration is performed in two steps, the first of which proceeds along a straight line from some upstream position to the leading edge of the airfoil, and the latter continues then along the airfoil contour from the leading edge to the midpoint of each panel.

The setup for the next timeline requires the convection of the singularities within the wake. The free point vortices of the wake are carried with the fluid as if they were fluid particles. The distributed vorticity along the wake element is first concentrated into a single point vortex, and then convected from the midpoint of the wake element in the same fashion. The path of each particle is obtained by a single step integration procedure (predictor step only), which approximates the actual path by short pieces of straight lines that are tangent to the actual path

$$\begin{Bmatrix} X_m(t_{k+1}) \\ Y_m(t_{k+1}) \end{Bmatrix} = \begin{Bmatrix} X_m(t_k) \\ Y_m(t_k) \end{Bmatrix} + (\vec{V}_m)_k (t_{k+1} - t_k) \quad (2.16)$$

This completes the formulation and description of the method to solve the inviscid part of the flow over an airfoil that is executing some kind of time-dependent motion. For further details, like the calculation of the influence coefficients, the reader is referred to Teng (thesis at NPS /42/).

3. The unsteady boundary layer method

Introduction

For many flows of aerodynamic interest the Reynolds number is large enough such that the flowfield can be divided into two regions: an inner region, which consists of the boundary layers along the wall and in the wake, and an outer inviscid region. The flow within the inner region is assumed to be governed by Prandtl's boundary layer equations, which constitute one of the asymptotic approximations to the Navier-Stokes equations for large Reynolds numbers. The Navier-Stokes equations are thought of as the exact equations of motion for a viscous fluid. Furthermore the full equations (which are written in instantaneous flow quantities) apply equally to laminar and turbulent flows. Though the full Navier-Stokes equations would resolve every detail of the turbulent motion (no matter how small the scale is chosen), their solution is, at the present time, not seriously considered for engineering purposes because of costs. In order to solve turbulent flows for applied problems the time-accurate equations are replaced by time-averaged equations. This is accomplished by time-averaging the turbulent fluctuations over a time-scale that does not resolve any details of the turbulent motion, yet is small enough to describe every detail of the mean flowfield. Virtually all engineering methods pursue this approach, that is the solution of the Reynolds-averaged Navier-Stokes equations or of some asymptotic approximation to them. It is owing to Prandtl, that the Navier-Stokes equations had been reduced to a much simpler form opening the way to a wide range of methods, that enable to account for viscous effects in a simple fashion. Prandtl's boundary layer concept derives from the assumption that changes in the velocity (within the viscous layer) occur more rapidly across the layer than along it. The larger gradient of the velocity in the cross-stream direction can be explained by means of the no-slip condition, which requires that fluid particles on the airfoil contour must not move with respect to it. Consequently, there is only a thin layer left, in which the particles shall change their velocity from zero to the external frictionless velocity. Such a layer is referred to as a boundary layer, or (using the more recent terminology) as a thin shear layer.

The nature of the flow in a boundary layer differs considerably from that of Navier-Stokes governed flows. Whereas the Navier-Stokes equations provide a mechanism such that disturbances get carried in all directions, the boundary layer equations put some limitations on that process. Foremost, the streamwise diffusion, as encountered in Navier-Stokes governed flows due to viscous and turbulent stress gradients, does not take place in boundary layers. Furthermore, there are no pressure signals propagating within the boundary layer, because the pressure is imposed from outside. This gives rise to a flowfield, in which the flow is uninfluenced by downstream events. Such a behavior is, mathematically speaking, termed parabolic. From a numerical point of view, the parabolic behavior is one of the biggest assets of the boundary layer equations, since parabolic equations admit marching algorithms. These algorithms obtain a solution by proceeding step by step in the marching direction such that the solution at a particular point is made dependent on the results of already computed steps only. The unsteady boundary layer equations offer two of these directions, namely the streamwise direction and time. The presented methodology takes advantage of both: For a given time level the procedure performs a sweep for each the upper and the lower surface, with the solution of each sweep advancing step by step from the stagnation point towards the trailing edge. After a complete solution of a particular time level has been obtained, the scheme proceeds to the next time level and the described routine is repeated. Accordingly, a single step will yield the solution for a column of points at a given streamwise position and for a given time. In contrast to the stepwise advancing of

the solution in the streamwise direction and in time, the solution for such a column must be attempted simultaneously in order to account for the viscous diffusion in the cross-stream direction. Each step adds another column to the already computed flow solutions such that the field (x, t -plane) is successively covered by those columns. The efficiency of the boundary layer approach derives from this algorithm of marching solutions, which bypasses the laborious field solution as required by the Navier-Stokes equations.

While the boundary layer approach represents a very economic means of computing viscous flows, it is not a universal tool. The boundary layer equations do apply only to flowfields, which satisfy the assumption on which the boundary layer approximation is based. That is the condition that viscosity affects the flow essentially only in a very thin layer. This assumption excludes flowfields experiencing a massive separation, like the flows past blunt bodies or the flows past streamlined bodies at high angles of incidence. Further, because the pressure is imposed on the boundary layer by the outer flow, the classical boundary layer approach is not applicable in regions, where the viscous layer has a substantial effect on the pressure. As far as the boundary layer is concerned, the pressure is a known function of the streamwise coordinate and of time. The pressure ceases to be a function of the cross-stream coordinate and hence remains constant across the boundary layer. Because of this the boundary layer approach cannot cope with flows past bodies, whose surface curvature either is large or changes abruptly. In spite of all these limitations Prandtl's boundary layer concept proves extremely useful in analysing viscous flows because of the substantial simplifications achieved by reducing the originally governing Navier-Stokes equations.

The differential equations, the boundary and initial conditions

The boundary layer equations can be obtained by applying an order of magnitude analysis to the Navier-Stokes equations. Utilizing Prandtl's finding, that the thickness of the viscous layer is small compared to a characteristic length in the primary flow direction, the magnitudes of the terms in the Navier-Stokes equations can be estimated. Keeping only those terms of the largest order of magnitude leads to Prandtl's famous set of boundary layer equations (see for example [37]). The time-dependent boundary layer equations for two-dimensional, incompressible flow take in terms of dimensional variables the following form

$$\frac{\partial u}{\partial x} + \frac{\partial v}{\partial y} = 0 \quad (3.1)$$

$$\frac{\partial u}{\partial t} + u \frac{\partial u}{\partial x} + v \frac{\partial u}{\partial y} = \frac{\partial u_e}{\partial t} + u_e \frac{\partial u_e}{\partial x} + v \frac{\partial}{\partial y} \left(b \frac{\partial u}{\partial y} \right) \quad (3.2)$$

The foregoing equations are subject to the usual boundary conditions, which are the no-slip condition on the airfoil contour and the prescription of the external velocity at the outer edge of the boundary layer

$$\begin{aligned} y = 0: & \quad u = v = 0 \\ y \rightarrow \infty: & \quad u \rightarrow u_e(x, t) \end{aligned} \quad (3.3)$$

Here the b denotes a scaled viscosity such that the equations apply equally to the laminar and turbulent regimes. Its turbulence related contribution must be provided by a turbulence model, which, in our scheme, is based upon the eddy viscosity concept. All flow variables represent ensemble averages over a large enough time, such that the above equations need not describe the turbulent fluctuations. The equations are expressed in curvilinear coordi-

nates x and y , which are directed along and normal to the airfoil contour, and in the velocity components u and v along these directions. The pressure gradient in x -direction is written in terms of the tangential velocity component of the external flow, which, to a first approximation, may be assumed identical to the frictionless flow past the airfoil. Consequently the external velocity distribution is obtained from an unsteady panel method, which solves for the (inviscid) potential flow past the airfoil.

In order to complete the formulation of the problem, initial conditions must be prescribed for the entire x, y -plane at some initial time t_i , as well as upstream boundary conditions for the entire t, y -plane at some initial section x_s ,

$$\begin{aligned} t = t_i \quad \text{and} \quad x \geq x_s: \quad u = u_i(x, y) \\ x = x_s \quad \text{and} \quad t > t_i: \quad u = u_s(y, t) \end{aligned} \quad (3.4)$$

On the assumption that steady flow conditions prevail at the time t_i , the initial conditions can be obtained from a steady-state solution of the boundary layer equations. Further, it is assumed that the unsteady motion develops gradually ($\partial u / \partial t = 0$ at t_i), such that double structured boundary layers need not be considered. The upstream boundary conditions require the prescription of a velocity profile at the stagnation point for $t > t_i$. While the generation of the upstream boundary conditions does not present any problems for steady-state flows (recall that the velocity profile at the steady stagnation point can be derived from a similarity solution), this undertaking proves much more difficult in the case of unsteady flows. First, because the tangential velocities at the stagnation point in unsteady flows do no longer vanish across the layer, as they do in steady flows, and second, because of the possible occurrence of flow reversals at the unsteady stagnation point. The details of the procedure that can cope with both problems are given in Appendix C. In summary, the procedure consists of an iterative computation of the flow at the stagnation point, and the adjacent upper and lower surface points. In particular, the computation of the flow at the stagnation point involves the use of a modified characteristic box scheme, which differs in that the momentum and continuity equations are solved successively and in a decoupled manner. In closing this paragraph it seems appropriate to point out, that only differential equations that are accompanied by suitable initial and boundary conditions constitute a mathematically well posed problem.

Signal propagation in unsteady boundary layers

The discretization of the just established, unsteady boundary layer problem shall be described next. Formally, the partial differential equations are approximated by finite difference equations, which can be found through the use of Taylor-series expansions. Though such an approximation will be consistent with the exact equations (in the sense that in the limit of an infinitely small meshsize the truncation error of the approximation tends towards zero), it just might not work. The necessary - and in case of a linear equation sufficient - condition for a numerically converging scheme is stability. Stability means here the capability of the scheme to dampen errors of any source while advancing from one marching step to the next. From a physical point of view even such a scheme might be faulty. A physically sound scheme needs, in addition, to incorporate the mechanism of signal propagation as imposed by the differential equation. In the following we will elaborate on this process and its consequences on the design of a finite difference method.

The unsteady boundary layer equation is characterized by two well known types of signal propagation: Regarding the streamwise velocity u as a function of x, y as well as of y, t the equation is diffusive, whereas regarding u as a function of x, t it behaves like a wave

equation. Consequently, the unsteady boundary layer equation contains two time-like initial-value variables, namely the streamwise coordinate x and the time t , and one boundary-value space variable, namely the boundary layer coordinate y . How does this relate to the mechanism through which information is transmitted in an unsteady boundary layer? Let us assume that a slight disturbance is generated at the point (x_1, y_1, t_1) and let us trace its route. In the very instant the disturbance is generated, it propagates immediately across the boundary layer station (x_1, t_1) , that is along the line $x = x_1$ and $t = t_1$ all the way down to the wall and up to the edge of the boundary layer. In a local perspective information also travels along the streamlines with the speed of convection. But globally this process adds up to a streamwise transport of information with $\max(u)$ and $\min(u)$ as the velocities of propagation. This is readily explained. The disturbance instantly diffuses to all layers of the station (x_1, t_1) , from where it continues its path in each of these layers ($y = \text{constant}$ planes) with the local particle speed u . As soon as the signal reaches a new station (x_2, y_2, t_2) , the signal there immediately spreads to all values of y at that station. Because of this mechanism the signal effectively travels with the maximum velocity in the downstream direction, and in case of a flow reversal with the maximum backflow velocity in the upstream direction. Thus the mode of propagation in the streamwise direction is as follows: The signal travels up to the edge of the boundary layer in the instant of its generation, and then travels through the outmost part of the boundary layer with the speed of the external flow, which carries the signal downstream at the fastest speed possible. At each new station the signal is felt instantaneously across the layer because of the viscous diffusion in y -direction. There are no signals propagating upstream if there are no flow reversals. In case there are, signals follow a pattern similar to the downstream propagation, with the maximum reversed flow velocity taking the role of the external flow velocity.

As a consequence of the above outlined mechanism, the flow at a particular point does not depend on the entire flowfield, not even on the entire upstream flowfield. The formal tool to describe the flow of information is the concept of the zones of dependence and influence. They are defined as the zone whose points - and only whose points - do affect the flow at a particular point, and as the zone whose points - and only whose points - can be reached by signals sent from a particular point. For the unsteady boundary layer equations the zone of dependence (zone of influence) is a wedge-shaped volume (in the x, y, t -space), which is generated by two planes that are perpendicular to the x, t -plane and that include the outermost directions of all particle paths (projected in x, t -planes) across the boundary layer. These two directions correspond to the maximum streamwise velocity, which is usually the external velocity, and the minimum streamwise velocity, which is either zero or the largest reversed flow velocity

$$\begin{aligned} \frac{dx_1}{dt} &= \min_{0 \leq y \leq \delta} [u(x, y, t)] = -\max_{0 \leq y \leq \delta} |u_{rev}| \quad (= 0) \\ \frac{dx_2}{dt} &= \max_{0 \leq y \leq \delta} [u(x, y, t)] = \max_{0 \leq y \leq \delta} |u| \quad (= u_e) \end{aligned} \quad (3.5)$$

The implications of these findings regarding the layout of the finite difference scheme are usually summarized in two rules: the dependence rule and the law of forbidden signals. The former one requires that the computational domain of dependence brackets the domain of dependence as defined by the differential equation. This rule is occasionally linked to the ubiquitous Courant-Friedrichs-Lewy condition /15/, which as it is argued, can be interpreted geometrically in such a way. While that is true for the original CFL-condition, which is the stability criterion of explicit schemes for solving linear hyperbolic equations, the generalization to parabolic problems and implicit schemes does not hold good. In general, the stability constraint may not coincide with the condition resulting from the dependence

rule. In fact, schemes have been reported that do satisfy the dependence rule and are inherently unstable /28/. The second rule, the law of forbidden signals, is rarely recognized and it is violated in most schemes currently used. This law postulates that numerical schemes shall prohibit the reception of signals that cannot exercise any influence, because they do not originate within the zone of dependence as defined by the differential equation. Thus the dependence rule and the law of forbidden signals lead to contradictory statements, though both are motivated by the proper implementation of the physics. Well, there is a scheme possible that can satisfy both rules, namely one in which the computational domain of dependence and that one defined by the differential equation do coincide. For now the objective is to find a scheme that implements these principles as well as possible under the constraint of stability and in consideration of the limited computer resources available.

The numerical procedure

The numerical solution of the unsteady boundary layer equations is obtained with a technique that utilizes both the regular box scheme and the characteristic box scheme. The box method was devised by Keller /25/ for solving diffusion problems, and has, since then, extensively been applied to a wide variety of parabolic problems /26/, with particular success to boundary layer flow problems. One of the strongest advocates of the box method has been (and is) Cebeci, who, together with his collaborators /3,10,11/, has contributed a good deal of the techniques associated with this method. The differencing of the box method is implicit with respect to the cross-stream direction, and second order accuracy is formally granted in time and both space coordinates on arbitrary, nonuniform nets. The box method is said to be unconditionally stable, even with the use of a large meshsize and the appearance of rapid net variations.

After this brief introduction of the box method, we focus on the peculiarities of the unsteady approach, in particular in comparison with the well-established steady box method. Though the unsteady boundary layer equations differ from their steady counterparts only by the appearance of the time-derivative $\partial u/\partial t$, the concepts of solution for steady flows do not directly carry over to unsteady flows. This is not so much because of the additional dimension, rather than because of the different nature of the equations. In this regard the unsteady, 2-dimensional equations are much closer related to the steady, 3-dimensional equations. The thread between the two of these is the common mechanism of signal propagation, which, in turn, is instrumental to the choice of the finite difference representation. The essential feature, missing in practically all steady, 2-dimensional procedures, is the, for unsteady, 2-dimensional and steady, 3-dimensional flows absolutely crucial, incorporation of upstream influence. The presented technique takes this fully into account by switching from the regular to the characteristic box scheme /8/ as soon as the streamwise velocity indicates backflow. The characteristic box scheme admits the indispensable upstream influence by expressing the governing equations with respect to those directions, along which disturbances in the x, t -plane are locally propagated. The integral curves of these directions are defined by

$$\frac{dx(s)}{ds} = u \frac{dt(s)}{ds} \quad (3.6)$$

where s denotes the coordinate along such a curve. The method owes its name to the concept of characteristics, which is well known in the theory of hyperbolic equations, but also is intimately linked to the mechanism of signal propagation. The above addressed paths, along which disturbances are locally convected, are associated with so-called subcharacteristics. (These are characteristics of a simplified problem, in which the highest derivatives of

the original problem, in our case the viscous diffusion term, are neglected. For a more elaborate explanation see for example reference /40/.) The characteristic method uses then differencing along the subcharacteristic direction

$$\frac{\partial}{\partial t} + u \frac{\partial}{\partial x} = \frac{d}{dt} \Big|_{s=\text{const}} = \frac{1}{dt(s)/ds} \frac{d}{ds} \quad (3.7)$$

such that the momentum equation can be reformulated as

$$\frac{1}{dt(s)/ds} \frac{du}{ds} = -v \frac{\partial u}{\partial y} + \frac{\partial u_e}{\partial t} + u_e \frac{\partial u_e}{\partial x} + v \frac{\partial}{\partial y} \left(b \frac{\partial u}{\partial y} \right) \quad (3.8)$$

The significance of this equation is that its solution corresponds formally to an integration of the right hand side along the subcharacteristic curve. This circumvents the difficulties encountered when the regular method is employed in regions of reversed flow.

Before we continue with the details of the box method, we introduce a coordinate transformation. Most of the boundary layer methods employ scaled variables in order to reduce the rapid variation that occurs near the wall. Numerically it is advantageous to deal with quantities of the same order of magnitude. To this end the dependent variables are nondimensionalized by a reference length L and a reference speed U_∞ , which in the actual calculation are taken as the chordlength and the freestream velocity, respectively

$$\xi = \frac{x}{L}, \quad \eta = \sqrt{R_L} \frac{y}{L}, \quad \tau = \frac{U_\infty}{L} t \quad (3.9)$$

where the Reynolds number R_L is defined in terms of the reference scales

$$R_L = \frac{U_\infty L}{\nu} \quad (3.10)$$

Not accidentally the normal coordinate is stretched by a factor involving the squareroot of the Reynolds number. It is one of the first and simplest results of boundary layer theory, that the boundary layer thickness is proportional to $1/\sqrt{R_L}$. Thus the newly defined, normal coordinate η will be of the same order as the streamwise coordinate. This particular coordinate transformation (yielding so-called physically transformed coordinates) is not as powerful as other commonly used transformations, say for example the Falkner-Skan transformation. It does neither maintain a constant boundary layer thickness nor eliminate the stagnation point singularity, as the Falkner-Skan transformation is able to. The reason for introducing such a simple transformation lies to some extent in the necessities dictated by the unsteady formulation of the box method.

The solution of the boundary layer equations by the box method involves four steps, of which the first is discussed later in this section, the second and third are described in Appendices A and B, and the fourth must be looked up elsewhere (for example in any textbook by Cebeci /3,6/). The four steps are:

1. The boundary layer equations are reduced to a system of first order differential equations.
2. The first order differential equations are approximated by simple centered differences and two-point averages, using values at the corners of one difference molecule only.
3. The resulting algebraic equations are linearized by Newton's method.
4. Finally, the numerical solution of the resulting block tridiagonal system is carried out by the block elimination method.

The first step of the box method is in order to allow the approximation of all functions and derivatives in terms of the quantities at the corners of one difference molecule only. To this end a new dependent variable, V , is introduced to eliminate the second order derivatives in the momentum equation. Using the scaled velocities U and F , the scaled vorticity V , as well as the scaled external velocity W

$$U = \frac{u}{U_\infty}, \quad V = \frac{1}{\sqrt{R_L}} \frac{L}{U_\infty} \frac{\partial u}{\partial y}, \quad F = -\sqrt{R_L} \frac{v}{U_\infty}, \quad W = \frac{u_e}{U_\infty} \quad (3.11)$$

the boundary layer equations can be rewritten as a system of three first order differential equations

$$\frac{\partial U}{\partial \xi} - \frac{\partial F}{\partial \eta} = 0 \quad (3.12)$$

$$\frac{\partial}{\partial \eta} (bV) + FV - \frac{\partial U}{\partial \tau} - U \frac{\partial U}{\partial \xi} = -\frac{\partial W}{\partial \tau} - W \frac{\partial W}{\partial \xi} \quad (3.13.a)$$

$$\frac{\partial}{\partial \eta} (bV) + FV - \sqrt{1+U^2} \frac{\partial U}{\partial s} = -\frac{\partial W}{\partial \tau} - W \frac{\partial W}{\partial \xi} \quad (3.13.b)$$

$$V = \frac{\partial U}{\partial \eta} \quad (3.14)$$

The first of these equations refers to the conservation of mass, the second and the third represent the conservation of momentum either in regular or in characteristic form, and the fourth defines the extra variable. Equations (3.13.a) and (3.13.b) are used alternately, depending on the sign of the local streamwise velocity. The foregoing equations are complemented by boundary conditions, requiring no slip at the wall and matching of a prescribed velocity at the edge of the boundary layer

$$\begin{aligned} \eta = 0: \quad U = F = 0 \\ \eta = \eta_e: \quad U = W(\xi, \tau) \end{aligned} \quad (3.15)$$

When completed by a closure relationship for the turbulent shear stresses (see following section), by appropriate initial and upstream boundary conditions (see preceding section and Appendix C), the problem is all set for the numerical solution. For the details of the further proceeding the reader is referred to Appendix A for the regular and Appendix B for the characteristic box method.

Before we close this section, we would like to comment on a practical and a hypothetical aspect of the solution procedure. The practical implementation of the regular box scheme required a modification of the commonly used procedure. The modification was necessitated by the occurrence of streamwise oscillations in the near-wall solutions. An analysis of this instability, together with the outline of the modification, is given in Appendix E. The comment on the hypothetical aspect deals with the question how well the box method satisfies the dependence rule and the law of forbidden signals. Following the explanations of the preceding section the domain of dependence is a wedge-shaped volume, which is generated by two planes that touch the outermost subcharacteristics. The dependence rule requires that information be included from all points located between those two planes. While the characteristic box method attempts to simulate the local mechanism of signal propagation, and it succeeds in that by formulating the momentum equation along the path a disturbance would take in a local perspective, it fails to reproduce the global mechanism. The characteristic box scheme includes information from a single point only, namely the

origin of the subcharacteristic on the previous timeline, whereas all points between the two outermost subcharacteristics should be included. Consequently the characteristic box method is seen to violate the dependence rule, though not to a dramatic extent. On the other hand, the characteristic scheme certainly satisfies the law of forbidden signals. Notably, the regular box method does not. Information on the same timeline, that is included in the regular scheme, is not only undue, but physically impossible, since signals do not spread with infinite speed in the streamwise direction. Finally, it should be pointed out, that the technique of regular and characteristic boxes probably reproduces the mechanism of signal propagation better than any other method.

Turbulence modeling and transition

In order to solve the boundary layer equations for the turbulent flow regime, the governing differential equations must be completed by a closure relationship for the apparent turbulent shear stress. This term has been added to the equations in the process of averaging the time-accurate equations, which is in order to bypass the extremely costly calculation of the turbulent fluctuations. Furthermore, from the engineer's point of view the computation of the turbulent motion beyond a certain time- and length-scale seems unnecessary, since the main focus is on the mean flow. The averaged equations combined with a turbulence model represent then, hopefully, a less complicated set of equations. Turbulence modeling consists of providing suitable means for the approximation of the turbulent shear stresses. Most of today's models fall into two categories: those which are based upon the eddy viscosity hypothesis, and those which solve one or more Reynolds stress transport equations. Both types of models involve empirical constants and hence require a verification by comparison with experimental data. Establishing a relationship between the unknown turbulent shear stresses and the mean flow variables closes the set of Reynolds-averaged equations in that the number of unknowns is reduced to equal the number of equations.

Today there is a wide variety of turbulence models available, ranging from the simple algebraic eddy viscosity models to the sophisticated stress-equation models. The classification of models is according to the number of the partial differential equations, that are involved in the calculation of the shear stresses. Though the more complex models, including the widely used $k-\epsilon$ model, promise more generality, it is not obvious that their accuracy is superior to simple models. The most common approach (in engineering calculations) adopts Boussinesq's concept of eddy viscosity (1877), in which the apparent turbulent shear stress is assumed to be related to the rate of mean strain through a turbulent (eddy) viscosity

$$\frac{\tau}{\rho} = \frac{\tau_l + \tau_t}{\rho} = \nu \frac{\partial u}{\partial y} - \overline{u'v'} = (\nu + \nu_t) \frac{\partial u}{\partial y} = \nu_b \frac{\partial u}{\partial y} \quad (3.16)$$

This model simply adds a turbulence related viscosity to the laminar viscosity. The strengths of the concept are its simplicity and the convenience of maintaining the same form of differential equations for laminar and turbulent flows. The major shortcomings of these models lie in that the turbulent viscosity is evaluated in terms of local flow parameters and in the need to separately tune the model for different classes of flows. In view of the engineering oriented purpose of our efforts, we decided in favor of such a simple model, in particular we use the algebraic eddy viscosity formulation of Cebeci and Smith /6/. This model, representing a zero-equation closure, evaluates the turbulent shear stress through an algebraic equation. The eddy viscosity is given by a two-layer model, whose inner region

is based on Van Driest's approach, and whose outer region is based on a velocity defect approach

$$\begin{aligned} v_t &= \left\{ 0.4 y \left[1 - \exp \left(-\frac{y}{A} \right) \right] \right\}^2 \left| \frac{\partial u}{\partial y} \right|_{\gamma_{tr}} & \text{for } 0 \leq y \leq y_c \\ v_t &= 0.0168 \left| \int_0^\infty (u_e - u) dy \right|_{\gamma_{tr}} & \text{for } y_c \leq y \leq \delta \end{aligned} \quad (3.17)$$

where $A = 26\nu / \left(\nu \frac{\partial u}{\partial y} \right)_{\max}^{1/2}$

Here the crossover distance y_c is defined as the location where the eddy viscosities of inner and outer regions coincide. The presented model is essentially identical to the steady-state formulation. Originally, Cebeci and Smith did include some unsteady correction terms, which showed up in the damping constant A . In a previous investigation, however, the unsteady correction terms turned out to have little effect on the results [20]. Consequently in our computations these terms are not accounted for. Nevertheless, there is plenty of effects that require alterations to algebraic turbulence models. For example it is well known that transition is not an instantaneous process, and hence the transitional region ought not to be reduced to a switching point between the laminar and the turbulent regions. In order to account for the transitional flow region, we make use of the intermittency distribution by Chen and Thyson [14]

$$\gamma_{tr} = 1 - \exp \left[-\frac{u_e^3}{G_{\gamma_{tr}} \nu^2} R_{x_{tr}}^{-1.34} (x - x_{tr}) \int_{x_{tr}}^x \frac{d\xi}{u_e} \right] \quad (3.18)$$

where x_{tr} and $R_{x_{tr}}$ are the location of the onset of transition and the transition Reynolds number, respectively. The empirical factor $G_{\gamma_{tr}}$ exercises a major influence on the length of transition. The originally assigned value of 1200 is suited well for high Reynolds number flows, whereas flows at lower Reynolds numbers require reduced values of $G_{\gamma_{tr}}$. Modifications due to other effects, like surface roughness, freestream turbulence, or streamwise wall curvature, have, as of now, not been implemented in our code. Though algebraic eddy viscosity models have accumulated a remarkable record, extreme caution is advised when models are applied outside the range of flows, upon whose data the empirical constants are based.

Since flows past airfoils comprise laminar, transitional, and turbulent regimes, there is the need to predict the onset of transition. In spite of the unargued importance of the accurate prediction of transition, our understanding of that process is unsatisfactory and incomplete. The currently available methods include empirical data correlations, which relate the onset of transition to some mean flow parameter, and linear stability theory, in which transition is deduced from the amplification ratio of disturbances obtained from the solution of the Orr-Sommerfeld equation. The prediction of transition in our scheme is based on a combination of Michel's empirical data correlation [33] and Smith and Gamberoni's e^9 -method. According to Cebeci [6] the resulting expression is given by

$$R_{\theta_{tr}} = 1.174 \left(1 + \frac{22400}{R_{x_{tr}}} \right) R_{x_{tr}}^{0.46} \quad (3.19)$$

where $R_{\theta_{tr}}$ and $R_{x_{tr}}$ are the Reynolds numbers based on the momentum thickness and the streamwise coordinate at the onset of transition, respectively.

Unsteady separation and singularities

The subject of flow separation and the possible occurrence of a singularity incident thereto has had a long and controversial history. Separation is the flow phenomenon, which, according to Brown and Stewartson /4/, can be described verbally as follows: "Here the main stream, which has hitherto been in close contact with the body, suddenly, and for no obvious reason, breaks away, and downstream a region of eddying flow, ..., is set up." And Brown and Stewartson continue to quantify their description in that they define separation as the transition from an attached boundary layer, which confines the viscous effects to a layer of $O(R^{-1/2})$, to a detached boundary layer, where viscous effects are felt in layers further from the wall. However, neither of these definitions is suited for identifying the point of separation in practice. Thus a considerable number of separation criteria has been proposed, but their general applicability, including time-dependent and 3-dimensional flows, remains to be proven.

The question of ample importance is whether flow separation can be related to the occurrence of a singularity in an uninteracted boundary layer description. For a long time it was known that the classical boundary layer solution breaks down due to the appearance of the Goldstein singularity /22/ in steady flows. The singularity can mathematically be characterized by the nonexistence or nonuniqueness of the solution, or by the growth of some flow variable beyond all bounds. Clearly, the Goldstein singularity is not physical, and the Navier-Stokes equations have even been shown to be free of such a singularity. The singular behavior of the solution can rather be read as an exaggeration of the actual flow, and as such might indicate the need for another, more appropriate set of equations. The existence of a similar singularity in the classical, say uninteracted, unsteady boundary layer solutions has been the subject of numerous investigations with, in part, strongly contradictory findings. The controversy was settled by Van Dommelen and Shen /43/, who gave a numerical proof that a singularity will develop in the laminar boundary layer of an impulsively started cylinder within a finite time. Since on the one hand the existence of singularities in the classical boundary layer description has been proven, and on the other hand the actual flow is not known to exhibit a singular behavior, the question arises, why a certain description does develop a singularity, and how it can be removed. The appearance of a singularity is believed to be the consequence of solving incomplete equations, as well as of an incorrect choice of the external velocity distribution. The boundary layer simply must not be considered separately from the external inviscid flow. Instead, it is necessary to account for the mutual interaction between the boundary layer and the external flow. This led to the development of the interactive boundary layer methods, which were able to remove the Goldstein singularity in steady flows, and at least to delay the appearance of Van Dommelen's singularity in unsteady flows.

Though the interactive methods enabled the computation of (moderately) separated flows by means of the boundary layer approach, they did not contribute to the yet unsolved task of identifying the point of separation. While this is not a problem in steady flows, where the point of separation coincides with the point of zero wall shear, it presents a formidable task in unsteady flows. There, the point of zero wall shear will, in general, be neither singular nor identical with the point of separation. None of the thus far proposed unsteady separation criteria turned out to be easily implementable and at the same time universally applicable. The generalized Goldstein criterion, which suggests the coincidence of separation

and singularity, can only observe symptoms, and lacks the practicality of a definite correlation. The MRS-criterion (the acronym MRS stands for Moore /34/, Sears /38/, and Rott /36/) was deduced by analogy with a steady boundary layer along a moving wall. Unsteady separation is predicted at the point, at which the shearing stress and the velocity, with respect to a frame of reference moving with the speed of separation, simultaneously vanish. Aside from the doubts about the universality, the implementation of such a criterion seems next to impossible due to the a priori unknown speed of separation. The probably most promising, though as well not very practical, approach is by Wang /47/. His criterion is based on the analogy with the well-established separation criterion for steady, 3-dimensional flows. It requires the evaluation of so-called skin friction lines (these are integral curves whose slope equals the skin friction) in the x, t -plane. Wang then proposes unsteady separation at points, at which the skin friction lines coalesce, provided they do so at all. Because of the lack of experimental evidence the status of any unsteady separation criterion remains, for the time being, that of uncertainty. Obviously, further work, both of experimental and numerical nature, is needed to attain a clearer picture of unsteady flow separation.

4. Results and discussion

Using the technique discussed in the preceding sections, pilot calculations were performed in order to do a system checkout prior to developing the interactive version of the code. The reader is reminded of the interim status of this investigation, which permits to run the code in the direct mode only. For that reason the tedious procedure of a detailed comparison with experimental data has been saved for the final version of the code. The calculations conducted thus far refer to the unsteady flow past an airfoil undergoing a ramp-change in angle of attack. Results were obtained for a small series of cases, different in the Reynolds number, the initial and final angle of attack, and the time required for the pitch-up. The presented results are confined to a single case, which can be described as follows. A NACA 0012 airfoil changes its angle of attack according to the rule

$$\alpha(\tau) = \begin{cases} \alpha_i & \text{for } \tau < 0 \\ \alpha_i + (\alpha_f - \alpha_i) (3 - 2\tau/\tau_f) \tau^2/\tau_f^2 & \text{for } 0 \leq \tau \leq \tau_f \\ \alpha_f & \text{for } \tau > \tau_f \end{cases} \quad (4.1)$$

For the shown case the airfoil initially encounters a steady flow at zero incidence ($\alpha_i = 0$ deg), then pitches by 5 deg, and finally holds this angle ($\alpha_f = 5$ deg). The airfoil pivots on the leading edge, and the pitch-up motion takes the same time the airfoil needs to travel one chordlength ($\tau_f = 1$). A Reynolds number of 1 million was chosen and the transition constant G_{ν}'' was set equal to 120. To ensure a proper resolution of the spatial and temporal scales the following gridsizes were selected to be in effect for the pilot runs. The external inviscid flow is determined at 100 points distributed along the airfoil contour. Boundary layer profiles are computed at 90 streamwise stations on each of the upper and the lower surface. Each profile consists of 35 to 75 velocity vectors, depending on the boundary layer thickness. The grid in normal direction is self-adapting in that the code automatically figures whether to increase or to decrease the number of points across the layer. Both potential and boundary layer flows are determined at 200 discrete time-levels, of which the first 100 are distributed over the ramp, and the second 100 over the stationary part of the airfoil motion. The time step is further controlled by a CFL-like-condition, which, in case of a flow reversal, might enforce shorter time steps than chosen by the program. This constitutes roughly the input, which is provided to the program for each single case. There is other data, like tolerance and relaxation parameter, which is set in the code.

The graphic output of the program includes snapshots of the boundary layer velocity profiles and the pressure distributions at selected time-levels, carpet plots for the distributions of skin friction and integral boundary layer thicknesses, and a time history of characteristic points, like those of zero skin friction and the onset of transition. Figure 1 and its continuations illustrate the change in the velocity profiles and in the pressure distribution over the period the airfoil travels 5 chordlengths. The shown plots refer to the time instances, at which the airfoil has covered a distance of 0.0, 0.5, 1.0, 1.5, 2.0, 3.0, 4.0, and 5.0 chordlengths, respectively. This is indicated by a marker in the angle of attack history at the lower left corner of each plot. The upper parts of the plots show the streamwise velocities inside the boundary layer at various stations on the airfoil contour. Additionally, the locations of the begin and end of transition are marked by a circle to allow for an easy reading of the different flow regimes. Since the boundary layer thickness amounts to few percent of the chord at the most, the vertical scales of the velocity profiles are enlarged by a factor of 10. The pitch-up affects the boundary layer primarily in two ways: First, the transition on the upper surface is shifted toward the leading edge, whereas on the lower surface toward the trailing edge. Second, the boundary layer grows on the upper surface,

in particular in the aft portion of the airfoil. Corresponding to the shift of transition, the regions of laminar and turbulent flow get redistributed: The flow starts out with 40 percent laminar, 15 percent transitional, and 45 percent turbulent flow on both surfaces. When the flow settles again after the pitch-up, the upper surface shows 10 percent laminar, 5 percent transitional, and 85 percent turbulent flow, while the lower surface shows 80, 10, and 10 percent. Finally, there is also a good correlation between the type of flow and the shape of the velocity profiles (almost textbook-like). The turbulent profiles can be identified by the rapid flow acceleration taking place very close to the wall. In contrast, the laminar profiles exhibit a much slower, yet more persistent, flow acceleration. The lower parts of Figure 1 present the pressure distribution and the location of the stagnation point with respect to the airfoil contour. Suction is indicated by arrows pointing from the airfoil, pressure by arrows pointing to the airfoil. In the course of the pitch-up the suction on the upper surface becomes much stronger, the initially symmetric pressure around the stagnation point shifts to the lower surface, and the suction on the lower surface reduces to the static pressure of the freestream. The peculiar pressure rise just upstream of the trailing edge is due to the neglect of the displacement effect in the inviscid flow calculation. Both the results for the boundary layer and the inviscid pressure field considerably lag behind the motion. When the airfoil first reaches its final angle of attack, the boundary layer profiles and the pressure distribution are no way near their final, stationary values. Even after four extra traveled chordlengths the results are not perfectly steady, though they then have pretty much approached their final state.

The following series of five plots consists of carpet plots for the external velocity distributions, the distributions of skin friction, displacement thickness, and momentum thickness, and the intermittency distributions. The development of the inviscid velocities along the airfoil contour with respect to time is shown in Figure 2. What has been said for the pressure applies equally to the velocities. They are only reproduced here, because they represent the input for the boundary layer flow solver. The most important output of a boundary layer calculation is (for practical purposes) the distribution of skin friction. Only this information allows the evaluation of the viscous drag of a body. The coefficient of skin friction c_f is a measure of the viscous shearing stress at the wall in terms of the dynamic pressure and can be computed from the velocity profiles according to

$$c_f = \frac{\tau_w}{\frac{1}{2}\rho u_e^2} = \frac{\mu \left(\frac{\partial u}{\partial y} \right)_{y=0}}{\frac{1}{2}\rho u_e^2} = \frac{2}{\sqrt{R_L}} \frac{V_{\eta=0}}{W^2} \quad (4.2)$$

The variation of this coefficient with the chordwise distance and as a function of time is depicted in Figure 3. The key message of this figure consists in that the locus of transition exercises a predominant influence on the viscous flow results. More than everything else, transition shapes the development of skin friction. The steep increase in skin friction, which shows up in virtually every single curve of Figure 3, is associated with transition. This behavior is entailed by the higher velocities of fluid particles near the wall in turbulent boundary layers, as compared to laminar ones. The shifting of transition due to the pitch-up is reflected as well in the shifting of the ramp-type increase in skin friction. The curves for skin friction (and the other boundary layer results) do not go all the way up to the trailing edge. Stations, whose boundary layer thickness had exceeded a certain limit, had to be dropped from the calculation for stability reasons. Convergence problems, as experienced for the last two stations in the steady calculations, are attributed to the direct mode of the boundary layer code, which cannot cope with flow separations. It should be pointed out, however, that these flow separations only occur because of the neglect of the displacement effect in the inviscid calculation. The inclusion of this effect shall take care of the

unrealistic strong pressure rise just upstream of the trailing edge, and consequently avoid this kind of flow separation. The rapid growth of the boundary layer at the most downstream station is believed to be related to the incomplete posing of the problem in that no boundary conditions are prescribed over the reversed flow region at the downstream face of the computational domain.

That leads us to the ways of measuring the thickness of a boundary layer. Not only because of the ambiguity involved in the definition of a "linear" boundary layer thickness, integral thicknesses, based, for example, on the deficit of mass flow or momentum due to the presence of the boundary layer, have been introduced. The most commonly used measure for the boundary layer thickness is the so-called displacement thickness δ^* , which is defined as

$$\frac{\delta^*}{L} = \frac{1}{L} \int_0^\infty \left(1 - \frac{u}{u_e}\right) dy = \frac{1}{\sqrt{R_L}} \int_0^{n^*} \left(1 - \frac{U}{W}\right) d\eta \quad (4.3)$$

The displacement thickness can be interpreted as the distance by which the external streamlines are shifted outwards owing to the presence of the boundary layer. Figure 4 shows the variations of this thickness as a function of the chordwise distance and time. Transition also leaves visible marks on the development of the displacement thickness in that it is accompanied by a short cessation of the otherwise continuous growth of the displacement thickness. This is caused by the sudden entrainment of faster fluid particles into the regions close by the wall, associated with the first occurrence of turbulence. Not surprisingly, such a trend cannot hold very long, and particularly, the outer parts of the turbulent boundary layer begin to spread further into the initially inviscid flowfield. This can be seen in the resumed, now even stronger growth of the turbulent boundary layer shortly downstream of transition. While the uneven displacement of the flows on the upper and the lower surface is responsible for the loss of lift, as suffered in viscous flow compared to the inviscid one, there is another integral thickness that relates to the drag, exerted on a body in viscous flows. In a similar way the displacement thickness is based on the loss of mass flow, the loss of momentum in a boundary layer can be used to define a second integral thickness, the so-called momentum thickness θ

$$\frac{\theta}{L} = \frac{1}{L} \int_0^\infty \frac{u}{u_e} \left(1 - \frac{u}{u_e}\right) dy = \frac{1}{\sqrt{R_L}} \int_0^{n^*} \frac{U}{W} \left(1 - \frac{U}{W}\right) d\eta \quad (4.4)$$

The development of the momentum thickness distributions in time is illustrated in Figure 5. The historically substantiated importance of the momentum thickness has been reduced since the introduction of finite difference methods, because flow reversals need no longer be predicted by the shape factor. The last of the carpet plots refers to the development of the intermittency distributions, which is shown in Figure 6. The intermittency distribution accounts for the transitional flow region, which exists between the laminar and the fully turbulent flow regimes. The most striking effect in Figure 6 is the steepening of the intermittency distribution, when transition moves toward the leading edge, and the flattening, when transition moves toward the trailing edge. This corresponds to a shortening or a lengthening of the transitional flow region, respectively. Such a behavior is not surprising in view of the role the external velocity plays in the equation for the intermittency.

Figure 7 summarizes the flow results in terms of time histories for characteristic points. The presented information includes the points of zero skin friction, the transition points, and the stagnation point. The reader is reminded of two earlier stated findings: First, with the exception of steady flow, the point of zero skin friction does not coincide with the point of flow separation, and second, the occurrence of flow reversals is partly attributed to the

neglection of the displacement effect. Even though, the history of the zero skin friction points shows a rather interesting behavior. Recalling that the airfoil pivots on the leading edge, the downward motion of the aft portion of the airfoil should give rise to a decreased entrainment on the upper surface and an increased entrainment on the lower surface. This, in turn, results in an extension of the reversed flow region on the upper surface and in the disappearance of it on the lower surface during the pitch-up. Most remarkable is the behavior when the airfoil stops its rotation. The flow, that has gotten used to the effects of pitching, reacts to the loss of these effects correspondingly, namely with the reduction of the reversed flow region on the upper surface and the development of a flow reversal on the lower surface. Thereafter the flow slowly approaches the steady results with no flow reversal on the lower and 4 percent on the upper surface. As far as transition is concerned, the results for upper and lower surface primarily differ in the amounts they lag the airfoil motion. The transition point on the upper surface reaches its steady-state position way sooner than the transition point on the lower surface does. This is related to the resistance an originally turbulent boundary layer offers to the transitioning to the laminar regime.

Though the results demonstrate that the method can qualitatively predict the essential flow features, they do emphasize the need for including an interaction model. Further, in order to quantitatively validate the code, a comprehensive comparison with an experimental investigation, that provides extensive data of the boundary layer, will be necessary.

5. Concluding remarks

This report describes the first step towards the development of a viscous-inviscid interaction method for unsteady flows. Such methods require the successive solution of the external inviscid flow and of the viscous flow in the boundary layers, linked together by a suitable interaction model. Our work has progressed towards the completion of the inviscid and viscous components of the method such that in the present status the code can be run in the so-called direct mode, which involves the solution of the viscous and the inviscid flows according to the classical, uninteracted conception. The chosen methodology utilizes an unsteady panel method for the solution of the inviscid part of the flow, and a finite difference method for the viscous part of the flow. The panel method derives from the steady technique of Smith and Hess, but additionally accounts for the continuous shedding of vorticity into the trailing wake. The boundary layer method adopts Cebeci's technique of regular and characteristic boxes, which allows a stable integration of the unsteady boundary layer equations in presence of flow reversals. A large portion of this report is devoted to the description of these techniques, whereas only little room is given to the presentation and analysis of results. The findings of the limited testing of the code and the lessons learned during the development of the code can be summarized in the following, yet preliminary conclusions:

1. In view of the influence the locus of transition exercises on the viscous flow results, the modeling of transition becomes the key factor in the prediction of unsteady viscous flows. It seems at least doubtful, that a simplified model, like the currently used Michel criterion, can cope with such a challenge. On top of it, the numerical implementation of the steady Michel criterion proved difficult in the unsteady environment.
2. In case of an open region of reversed flow, the boundary layer exhibited rapid growth at the most downstream station. It is believed that this behavior is related to the incomplete posing of the problem. The presence of reversed flow over part of the downstream face of the computational domain necessitates the prescription of boundary conditions, corresponding to the upstream boundary conditions at the stagnation point, there as well. Such conditions are not known a priori.
3. The occurrence of streamwise oscillations in the near-wall solutions of the boundary layer demanded a modification of the original box method. Since the averaging, resulting from the centered discretization, was identified as the cause of the problem, the scheme was modified in that the solution is now taken midway between succeeding streamwise stations.
4. The technique of regular and characteristic boxes is believed to be faulty with regard to the dependence rule. The damage caused by not accounting for the proper domain of dependence can hardly be evaluated, if only because of the lack of a faultless reference scheme. The flawless implementation of the dependence principle would likely require the abandonment of the characteristic box scheme. In view of the unargued merits of this scheme, such a step requires particularly careful consideration.
5. Sufficient evidence has been found to endorse the argument that in boundary layers the concept of stability is separate from the dependence principle. This is not in contradiction with the original CFL-condition [15], which does imply such an identity, since the CFL-condition strictly applies to linear, hyperbolic equations only, which are solved by means of an explicit scheme.
6. Considering the magnitudes of the boundary layer thicknesses witnessed in the calculations thus far, the assumption, that the normal pressure gradient is negligible in the boundary layer, might not hold. The removal of such an assumption, however, would

mean to sacrifice the computational efficiency of the space-marching boundary layer approach.

A conceptual comparison with related studies does not reveal anything fundamentally new. The investigations of most relevance to our approach are those by Henkes and Veldman (on the breakdown of unsteady interacting boundary layer description /23/), and by Geissler (on unsteady separation under dynamic stall conditions /20/). With regard to the above addressed criticism, those two investigations do not do a better job either. Both "cheat" on transition: The former study deals with laminar flows only, the latter one assumes the onset of transition right at the stagnation point. Neither of the studies provides answers to the questions of open separation and the fulfillment of the dependence rule. In order to compute flow reversals Geissler adopts the zig-zag scheme, which, from a physical point of view, in our opinion is less favorable than the characteristic box scheme. For the same purpose Henkes and Veldman employ the Crank-Nicolson method with upwind-differencing of the streamwise convection term. Concerning the interactive coupling of the viscous and inviscid components of the flow, however, both Henkes and Veldman, and Geissler are one step ahead of us, since both have such a feature already included in their present codes. That brings us to the improvements, which we anticipate to achieve in the short term, and which, in a broader context, we believe are necessary to advance the current abilities of predicting viscous flows:

1. Our method will now be extended to include a full interaction model, which should then permit the calculation of (moderately) separated flows. This goal shall be accomplished in two steps: First, the potential flow solver must be modified to account for the displacement effect due to the presence of the boundary layer. Second, the boundary layer method must be adapted to allow for the unknown status of the external velocity in the calculation of the boundary layer profiles.
2. The second near-term goal of our efforts refers to an improved implementation of the dependence rule, as well as of the law of forbidden signals. Though such an endeavour might not be beneficial from a practical point of view, we consider it important to reconcile the numerics with the underlying physics.
3. The extension of the interactive boundary layer description to the wake will not only resolve the problems with the unknown, yet (in case of a flow reversal) necessary, downstream boundary conditions, but will also greatly advance the ability to handle separated flows.
4. There is a great need to improve the modeling of transition and turbulence. In the long term, only a thorough understanding of these two phenomena will lead to a more reliable prediction of viscous flows.

Acknowledgments

The work reported herein was supported by the Naval Air Systems Command under Contract N62271-86-M-0229. During the preparation of the report additional support was provided by the NASA Lewis Research Center under Contract N62271-87-M-0190. The author wishes to express his sincere appreciation to Prof. Platzer for his constant encouragement and his assistance throughout the course of this project. Further thanks are extended to Prof. Cebeci, for providing his computer programs and his continued interest.

6. List of references

1. Anderson, D.A., Tannehill, J.C., and Pletcher, R.H., *Computational Fluid Mechanics and Heat Transfer*, Hemisphere Publishing Corporation, 1984.
2. Basu, B.C. and Hancock, G.J., The Unsteady Motion of a Two-Dimensional Airfoil in Incompressible Inviscid Flow, *J. Fluid Mech.*, Vol. 87, No. 1, pp. 159-178, 1978.
3. Bradshaw, P., Cebeci, T., and Whitelaw, J.H., *Engineering Calculation Methods for Turbulent Flows*, Academic Press, New York, 1981.
4. Brown, S.N. and Stewartson, K., Laminar Separation, *Ann. Rev. Fluid Mech.*, Vol. 1, pp. 45-72, 1969.
5. Catherall, D. and Mangler, K.W., The Integration of the Two-Dimensional Laminar Boundary-Layer Equations Past the Point of Vanishing Skin Friction, *J. Fluid Mech.*, Vol. 26, pp. 163-182, 1966.
6. Cebeci, T., and Smith, A.M.O., *Analysis of Turbulent Boundary Layers*, Academic Press, New York, 1974.
7. Cebeci, T. and Carr, L.W., Prediction of Boundary-Layer Characteristics of an Oscillating Airfoil, NASA TM 81303, 1981.
8. Cebeci, T. and Carr, L.W., Computation of Unsteady Turbulent Boundary Layers with Flow Reversals, and Evaluation of Two Separate Turbulence Models, *Proc. Roy. Soc. London, Series A*, Vol. 380, pp. 291-304, 1982.
9. Cebeci, T., Unsteady Boundary Layers with an Intelligent Numerical Scheme, *J. Fluid Mech.*, Vol. 163, pp. 129-140, 1986.
10. Cebeci, T., Clark, R.W., Chang, K.C., Halsey, N.D., and Lee, K., Airfoils with Separation and the Resulting Wakes, *J. Fluid Mech.*, Vol. 163, pp. 323-347, 1986.
11. Cebeci, T., An Approach to Practical Aerodynamic Configurations, VKI Lecture Series on Computation of Three-Dimensional Boundary Layers Including Separation, Brussels, 1986.
12. Cebeci, T., Krainer, A., Simoneau, R.J., and Platzer, M.F., A General Method for Unsteady Stagnation Region Heat Transfer for Model Turbine Flows, NASA TM 88903, prepared for the 2nd Thermal Engineering Conference, Honolulu, Hawaii, 1987.
13. Cebeci, T., Platzer, M.F., Teng, N.G., Krainer, A., and Simoneau, R.J., Progress Towards the Development of an Inviscid Interaction Method for Unsteady Flows in Turbomachinery Cascades, Proceedings of the Fourth International Symposium on Unsteady Aerodynamics and Aeroelasticity of Turbomachines and Propellers, Aachen, FRG, 1987.
14. Chen, K.K. and Thyson, N.A., Extension of Emmons' Spot Theory to Flows on Blunt Bodies, *AIAA Journal*, Vol. 9, pp. 821-825, 1971.
15. Courant, R., Friedrichs, K.O., and Lewy, H., Ueber die partiellen Differenzgleichungen der mathematischen Physik, *Mathematische Annalen*, Vol. 100, pp. 32-76, 1928.

16. Cousteix, J., Three-Dimensional and Unsteady Boundary-Layer Computations, *Ann. Rev. Fluid Mech.*, Vol. 18, pp. 173-196, 1986.
17. Drela, M. and Thompkins, W.T., Investigation of Compressible Laminar, Boundary-Layer Solution Behavior at Separation Using a Displacement Thickness-Based Normal Scaling, In *Numerical and Physical Aspects of Aerodynamic Flows* (ed. T. Cebeci), Vol. 2, pp. 327-335, 1983.
18. Drela, M., A New Transformation and Integration Scheme for the Compressible Boundary Layer Equations, and Solution Behavior at Separation, MIT Gas Turbine and Plasma Dynamics Laboratory, GTL Report No. 172, 1983.
19. Elliot, J.W. and Smith, F.T., Dynamic Stall due to Unsteady Marginal Separation, *J. Fluid Mech.*, Vol. 179, pp. 489-512, 1987.
20. Geissler, W., Zum Problem der instationaeren Abloesung an schwingenden Profilen, DVFLR-AVA Bericht Nr. 232-87 J 3, Aerodynamische Versuchsanstalt Goettingen, 1987.
21. Giesing, J.P., Nonlinear Two-Dimensional Unsteady Potential Flow with Lift, *J. Aircraft*, Vol. 5, No. 2, pp. 135-143, 1968.
22. Goldstein, S., On Laminar Boundary Layer Flow near a Position of Separation, *Quart. J. Mech. Appl. Math.*, Vol. 1, pp. 43-69, 1948.
23. Henkes, R.A.W. and Veldman, A.E.P., On the Breakdown of the Steady and Unsteady Interacting Boundary-Layer Description, *J. Fluid Mech.*, Vol. 179, pp. 513-529, 1987.
24. Hess, J.L., and Smith, A.M.O., Calculation of Potential Flow about Arbitrary Bodies, *Progress in Aeronautical Sciences* (ed. Kuchemann), Vol. 8, pp. 1-138, 1964.
25. Keller, H.B., A New Difference Scheme for Parabolic Problems, In "Numerical Solution of Partial Differential Equations" (ed. Hubbard), Vol. 2, Academic Press, New York, 1971.
26. Keller, H.B., Numerical Methods in Boundary-Layer Theory, *Ann. Rev. Fluid Mech.*, Vol. 10, pp. 417-433, 1978.
27. Kim, M.J. and Mook, D.T., Application of Continuous Vorticity Panels to General Unsteady Incompressible Two-Dimensional Lifting Flows, *J. Aircraft*, Vol. 23, No. 6, pp. 464-471, 1986.
28. Kitchens Jr., C.W., Sedney, R., and Gerber, N., The Role of the Zone of Dependence Concept in Three-dimensional Boundary-Layer Calculations, *Proceedings of the AIAA 2nd Computational Fluid Dynamics Conference*, Hartford, Connecticut, 1975.
29. Le Balleur, J.C. and Girodroux-Lavigne, P., A Viscous-Inviscid Interaction Method for Computing Unsteady Transonic Separation, In *Numerical and Physical Aspects of Aerodynamic Flows*, (ed. T. Cebeci), Vol. 3, 1986.
30. Lorber, P.F. and Carta, F.O., Unsteady Stall Penetration Experiments at High Reynolds Number, United Technologies Research Center, Report R87-956939-3, 1987.
31. Lorber, P.F. and Carta, F.O., Airfoil Dynamic Stall at Constant Pitch Rate and High Reynolds Number, AIAA Paper 87-1329, presented at the 19th AIAA Conference on Fluid Mechanics, Plasma Dynamics, and Lasers, Honolulu, Hawaii, 1987.

32. McCroskey, W.J. and Pucci, S.L., Viscous-Inviscid Interaction on Oscillating Airfoils in Subsonic Flow, *AIAA Journal*, Vol. 20, No. 2, pp. 167-174, 1982.
33. Michel, R., Etude de la transition sur les profils d'aile: établissement d'un critere de determination de point de transition et calcul de la trainee de profile incompressible, ONERA Rep. 1/1578A, 1951.
34. Moore, F.K., On the Separation of the Unsteady Laminar Boundary Layer, In *Boundary Layer Research* (ed. H. Goertler), Springer Verlag, pp. 296-311, 1958.
35. Peyret, R. and Taylor, T.D., *Computational Methods for Fluid Flow*, Springer Verlag, 1983.
36. Rott, N., Unsteady Viscous Flow in the Vicinity of a Stagnation Point, *Quart. J. Appl. Math.*, Vol. 13, pp. 444-451, 1956.
37. Schlichting, H., *Boundary-Layer Theory*, 7th Edition, McGraw-Hill, 1979.
38. Sears, W.R., Some Recent Developments in Airfoil Theory, *J. Aero. Sci.*, Vol. 23, pp. 490-499, 1956.
39. Smith, F.T., Steady and Unsteady Boundary-Layer Separation, *Ann. Rev. Fluid Mech.*, Vol. 18, pp. 197-220, 1986.
40. Stewartson, K., The Theory of Unsteady Laminar Boundary Layers, *Adv. in Appl. Mech.*, Vol. 6, pp. 1-37, 1960.
41. Telionis, D.P., *Unsteady Viscous Flows*, Springer Verlag, 1981.
42. Teng, N.G., The Development of a Computer Code (U2DIIF) for the Numerical Solution of Unsteady, Inviscid, and Incompressible Flow Over an Airfoil, M.S. Thesis, Department of Aeronautics, Naval Postgraduate School, 1987.
43. Van Dommelen, L.L. and Shen, S.F., The Spontaneous Generation of the Singularity in a Separating Laminar Boundary Layer, *J. Comp. Phys.*, Vol. 38, pp. 125-140, 1980.
44. Van Dommelen, L.L. and Shen, S.F., The Genesis of Separation, In *Numerical and Physical Aspects of Aerodynamic Flows* (ed. T. Cebeci), Vol. 1, pp. 293-311, 1982.
45. Veldman, A.E.P., New Quasi-simultaneous Method to Calculate Interacting Boundary Layers, *AIAA Journal*, Vol. 19, No. 1, pp. 79-85, 1981.
46. Wang, K.C., Aspects of "Multitime Initial-Value Problem" Originating from Boundary Layer Equations, *The Physics of Fluids*, Vol. 18, No. 8, pp. 951-955, 1975.
47. Wang, K.C., On the Current Controversy about Unsteady Separation In Numerical and Physical Aspects of Aerodynamic Flows (ed. T. Cebeci), Vol. 1, pp. 279-291, 1982.

Appendix A. The regular box scheme

This appendix provides detailed information on the discretization of the unsteady boundary layer equations by means of the regular box scheme. With the exception of reversed flow regions and the immediate neighborhood of the stagnation point, the regular box scheme is applied throughout the flowfield. The box method is a midpoint scheme, which expresses all functions or derivatives in terms of quantities at the corners of a computational cell. To this end the boundary layer equations are written as a system of three first-order partial differential equations

$$\frac{\partial F}{\partial \eta} - \frac{\partial U}{\partial \xi} = 0 \quad (A.1)$$

$$\frac{\partial}{\partial \eta} (bV) + FV - \frac{\partial U}{\partial \tau} - U \frac{\partial U}{\partial \xi} = - \frac{\partial W}{\partial \tau} - W \frac{\partial W}{\partial \xi} \quad (A.2)$$

$$\frac{\partial U}{\partial \eta} - V = 0 \quad (A.3)$$

This system is complemented by the usual boundary conditions, which are the no slip condition at the wall and the prescription of the external velocity at the boundary layer edge

$$\begin{aligned} \eta = 0: \quad U = F = 0 \\ \eta = \eta_e: \quad U = W(\xi, \tau) \end{aligned} \quad (A.4)$$

For the finite difference approximation a rectangular mesh with computational cells of size $r_i \times h_j \times k_n$ is introduced. The position in space and time is denoted by a treble suffix, for example $U_j^{i,n}$, where j is referring to the cross-stream direction, i to the streamwise direction, and n to the time. The equations can now be approximated in terms of central differences and two-point averages, involving the values at the corners of the computational cell only. Accordingly, the continuity equation (A.1) is evaluated at the point $(\xi_{i-1/2}, \eta_{j-1/2}, \tau_n)$, the momentum equation (A.2) at the center of the cell $(\xi_{i-1/2}, \eta_{j-1/2}, \tau_{n-1/2})$, and the auxiliary equation (A.3) at the point $(\xi_i, \eta_{j-1/2}, \tau_n)$

$$\frac{F_j^{i-1/2,n} - F_{j-1}^{i-1/2,n}}{h_j} - \frac{U_{j-1/2}^{i,n} - U_{j-1/2}^{i-1,n}}{r_i} = 0 \quad (A.5)$$

$$\begin{aligned} \frac{(bV)_j^{i-1/2,n-1/2} - (bV)_{j-1}^{i-1/2,n-1/2}}{h_j} + F_{j-1/2}^{i-1/2,n-1/2} V_{j-1/2}^{i-1/2,n-1/2} - \frac{U_{j-1/2}^{i-1/2,n} - U_{j-1/2}^{i-1/2,n-1}}{k_n} \\ - \frac{(U^2)_{j-1/2}^{i,n-1/2} - (U^2)_{j-1/2}^{i-1,n-1/2}}{2r_i} = - \frac{W^{i-1/2,n} - W^{i-1/2,n-1}}{k_n} - \frac{(W^2)^{i,n-1/2} - (W^2)^{i-1,n-1/2}}{2r_i} \end{aligned} \quad (A.6)$$

$$\frac{U_j^{i,n} - U_{j-1}^{i,n}}{h_j} - V_{j-1/2}^{i,n} = 0 \quad (A.7)$$

The boundary conditions read in terms of nodal values according to

$$\begin{aligned} U_1^{i,n} = 0, \quad F_1^{i,n} = 0 \\ U_j^{i,n} = W^{i,n} \end{aligned} \quad (A.8)$$

Since the resulting equations are algebraically nonlinear in the unknowns $U_j^{i,n}$, $V_j^{i,n}$, $F_j^{i,n}$, the scheme proceeds in linearizing the equations by Newton's method. This procedure approaches the solution in an iterative process, in which the variables of the κ th step are set equal the value of the previous iteration ($\kappa-1$) plus a small correction

$$\begin{aligned} U_j^{i,n,\kappa} &= U_j^{i,n,\kappa-1} + \delta U_j^{i,n,\kappa} & \text{where } \delta U_j^{i,n,\kappa} &\ll U_j^{i,n,\kappa-1} \\ V_j^{i,n,\kappa} &= V_j^{i,n,\kappa-1} + \delta V_j^{i,n,\kappa} & \text{where } \delta V_j^{i,n,\kappa} &\ll V_j^{i,n,\kappa-1} \\ F_j^{i,n,\kappa} &= F_j^{i,n,\kappa-1} + \delta F_j^{i,n,\kappa} & \text{where } \delta F_j^{i,n,\kappa} &\ll F_j^{i,n,\kappa-1} \end{aligned} \quad (A.9)$$

After dropping the terms involving quadratic expressions of the correction δ and collecting the like-terms, the unsteady boundary layer equations become

$$-\frac{1}{r_i} (\delta U_j^{i,n,\kappa} + \delta U_{j-1}^{i,n,\kappa}) + \frac{1}{h_j} (\delta F_j^{i,n,\kappa} - \delta F_{j-1}^{i,n,\kappa}) = (r_1^R)_j^{i,n,\kappa} \quad (A.10)$$

$$\begin{aligned} (s_1^R)_j^{i,n,\kappa} \delta V_j^{i,n,\kappa} + (s_2^R)_j^{i,n,\kappa} \delta V_{j-1}^{i,n,\kappa} + (s_3^R)_j^{i,n,\kappa} \delta F_j^{i,n,\kappa} + (s_4^R)_j^{i,n,\kappa} \delta F_{j-1}^{i,n,\kappa} \\ + (s_5^R)_j^{i,n,\kappa} \delta U_j^{i,n,\kappa} + (s_6^R)_j^{i,n,\kappa} \delta U_{j-1}^{i,n,\kappa} = (r_2^R)_j^{i,n,\kappa} \end{aligned} \quad (A.11)$$

$$\delta U_j^{i,n,\kappa} - \delta U_{j-1}^{i,n,\kappa} - \frac{h_j}{2} (\delta V_j^{i,n,\kappa} + \delta V_{j-1}^{i,n,\kappa}) = -(U_j^{i,n,\kappa-1} - U_{j-1}^{i,n,\kappa-1}) + h_j V_{j-1/2}^{i,n,\kappa-1} \quad (A.12)$$

This final set of algebraic equations is linear in the unknown corrections $\delta U_j^{i,n,\kappa}$, $\delta V_j^{i,n,\kappa}$, $\delta F_j^{i,n,\kappa}$. To avoid lengthy expressions equations (A.10) and (A.11) make use of the following abbreviations

$$\begin{aligned} (r_2^R)_j^{i,n,\kappa} = & - \left\{ \frac{b_j^{i,n} V_j^{i,n,\kappa-1} - b_{j-1}^{i,n} V_{j-1}^{i,n,\kappa-1}}{h_j} + \frac{(bV)_j^{i,n-1} - (bV)_{j-1}^{i,n-1}}{h_j} \right. \\ & + \frac{(bV)_j^{i-1,n} - (bV)_{j-1}^{i-1,n}}{h_j} + \frac{(bV)_j^{i-1,n-1} - (bV)_{j-1}^{i-1,n-1}}{h_j} \\ & + \frac{1}{4} (F_{j-1/2}^{i,n,\kappa-1} + F_{j-1/2}^{i,n-1} + F_{j-1/2}^{i-1,n} + F_{j-1/2}^{i-1,n-1}) (V_{j-1/2}^{i,n,\kappa-1} + V_{j-1/2}^{i,n-1} + V_{j-1/2}^{i-1,n} + V_{j-1/2}^{i-1,n-1}) \\ & - 2 \left[\frac{U_{j-1/2}^{i,n,\kappa-1} - U_{j-1/2}^{i,n-1}}{k_n} + \frac{U_{j-1/2}^{i-1,n} - U_{j-1/2}^{i-1,n-1}}{k_n} \right] \\ & \left. - \frac{(U^2)_{j-1/2}^{i,n,\kappa-1} + (U^2)_{j-1/2}^{i,n-1} - (U^2)_{j-1/2}^{i-1,n} - (U^2)_{j-1/2}^{i-1,n-1}}{r_i} \right\} \\ & - 2 \left[\frac{W^{i,n} - W^{i,n-1}}{k_n} + \frac{W^{i-1,n} - W^{i-1,n-1}}{k_n} \right] \\ & - \frac{(W^2)_j^{i,n} + (W^2)_j^{i,n-1} - (W^2)_{j-1}^{i-1,n} - (W^2)_{j-1}^{i-1,n-1}}{r_i} \end{aligned} \quad (A.13)$$

$$\begin{aligned}
(s_1^R)_j^{i,n,\kappa} &= \frac{b_j^{i,n}}{h_j} + \frac{1}{8} \left(F_{j-1/2}^{i,n,\kappa-1} + F_{j-1/2}^{i,n-1} + F_{j-1/2}^{i-1,n} + F_{j-1/2}^{i-1,n-1} \right) \\
(s_2^R)_j^{i,n,\kappa} &= -\frac{b_{j-1}^{i,n}}{h_j} + \frac{1}{8} \left(F_{j-1/2}^{i,n,\kappa-1} + F_{j-1/2}^{i,n-1} + F_{j-1/2}^{i-1,n} + F_{j-1/2}^{i-1,n-1} \right) \\
(s_3^R)_j^{i,n,\kappa} &= (s_4^R)_j^{i,n,\kappa} = \frac{1}{8} \left(V_{j-1/2}^{i,n,\kappa-1} + V_{j-1/2}^{i,n-1} + V_{j-1/2}^{i-1,n} + V_{j-1/2}^{i-1,n-1} \right) \\
(s_5^R)_j^{i,n,\kappa} &= -\frac{1}{k_n} - \frac{1}{r_i} U_j^{i,n,\kappa-1} \\
(s_6^R)_j^{i,n,\kappa} &= -\frac{1}{k_n} - \frac{1}{r_i} U_{j-1}^{i,n,\kappa-1} \\
(r_1^R)_j^{i,n,\kappa} &= -\frac{1}{h_j} \left(F_j^{i,n,\kappa-1} + F_j^{i-1,n} - F_{j-1}^{i,n,\kappa-1} - F_{j-1}^{i-1,n} \right) + \frac{2}{r_i} \left(U_{j-1/2}^{i,n,\kappa-1} - U_{j-1/2}^{i-1,n} \right)
\end{aligned} \tag{A.13}$$

Together with the boundary conditions equations (A.10) through (A.12) constitute a system of $3J$ algebraically linear equations (where J is the number of gridpoints across the boundary layer). The equations are arranged such that the resulting matrix is of the block-tridiagonal type. Each line of that matrix refers to a set of three equations (3×3 blocks)

1. The first set consists of the following equations
 - a. The boundary condition requiring zero tangential velocity at the wall
 - b. The boundary condition requiring zero normal velocity at the wall
 - c. The auxiliary equation (A.12)
2. Other than the first and last sets include the following
 - a. The continuity equation (A.10)
 - b. The momentum equation (A.11)
 - c. The auxiliary equation (A.12)
3. The last set is made up by the following three equations
 - a. The continuity equation (A.10)
 - b. The momentum equation (A.11)
 - c. The boundary condition prescribing the external velocity at the boundary layer edge

The solution of this system is obtained by the block elimination method, which consists of two sweeps. The forward sweep eliminates the blocks below the main diagonal. In the backward sweep the solution is calculated from recursion formulas. The actually employed method is specifically designed for the above described system, such that it is more efficient than a general algorithm for block tridiagonal systems.

Appendix B. The characteristic box scheme

This appendix deals with the difference approximation to the unsteady boundary layer equations by means of the characteristic box scheme. The characteristic box scheme was introduced by Cebeci and Stewartson in order to allow for some upstream influence when the local velocity is directed upstream. Consequently the characteristic box scheme is applied in regions of backflow and in the immediate neighborhood of the stagnation point. Further, the calculation of the upstream boundary conditions involves the iterative use of a modified characteristic box method, in which the continuity equation is decoupled from the momentum equation (see Appendix C.). In order to utilize the box scheme the unsteady boundary layer equations, with the streamwise convection term being evaluated along a subcharacteristic, are reduced to a system of first-order partial differential equations

$$\frac{\partial F}{\partial \eta} - \frac{\partial U}{\partial \xi} = 0 \quad (B.1)$$

$$\frac{\partial}{\partial \eta} (bV) + FV - \sqrt{1 + U^2} \frac{\partial U}{\partial s} = - \frac{\partial W}{\partial \tau} - W \frac{\partial W}{\partial \xi} \quad (B.2)$$

$$\frac{\partial U}{\partial \eta} - V = 0 \quad (B.3)$$

Here the newly introduced coordinate s denotes the distance along the subcharacteristic. Only the momentum equation (B.2) differs from that of the regular box scheme, while the continuity equation (B.1), the auxiliary equation (B.3), and the boundary conditions are identical to those of the regular box scheme. The discretization closely follows the procedure as given in Appendix A. The centering of the continuity and the auxiliary equations remains unchanged, namely the continuity equation is evaluated at the point $(\xi_{i-1/2}, \eta_{j-1/2}, \tau_n)$, and the auxiliary equation at the point $(\xi_i, \eta_{j-1/2}, \tau_n)$. The difference molecule for the momentum equation is here a rectangular plane, generated by the $\eta -$ axis and the direction of the subcharacteristic. Hence the momentum equation is centered at the midpoint of this rectangular plane, which is $(\xi_p, \eta_{j-1/2}, \tau_{n-1/2})$

$$\frac{F_j^{i-1/2,n} - F_{j-1}^{i-1/2,n}}{h_j} - \frac{U_{j-1/2}^{i,n} - U_{j-1/2}^{i-1,n}}{r_i} = 0 \quad (B.4)$$

$$\frac{1}{2} \left\{ \frac{(bV)_j^{i,n} - (bV)_{j-1}^{i,n}}{h_j} + \frac{(bV)_j^{m,n-1} - (bV)_{j-1}^{m,n-1}}{h_j} \right\} + \frac{1}{4} (F_{j-1/2}^{i,n} + F_{j-1/2}^{m,n-1}) (V_{j-1/2}^{i,n} + V_{j-1/2}^{m,n-1})$$

$$- \frac{1}{2} \left[\sqrt{1 + (U^2)_{j-1/2}^{i,n}} + \sqrt{1 + (U^2)_{j-1/2}^{m,n-1}} \right] \frac{U_{j-1/2}^{i,n} - U_{j-1/2}^{m,n-1}}{\Delta s_{j-1/2}^{p,n-1/2}} \quad (B.5)$$

$$= - \frac{W_{j-1/2}^{p,n} - W_{j-1/2}^{p,n-1}}{k_n} - \frac{(W_{j-1/2}^{i,n} + W_{j-1/2}^{m,n-1})(W_{j-1/2}^{i,n-1/2} - W_{j-1/2}^{m,n-1/2})}{2(\xi_i - \xi_m)}$$

$$\frac{U_j^{i,n} - U_{j-1}^{i,n}}{h_j} - V_{j-1/2}^{i,n} = 0 \quad (B.6)$$

The suffix m denotes the streamwise location where the subcharacteristic intersects the previous timeline. The station ξ_p is located halfway between ξ_i and ξ_m . Any flow quantity

which needs to be evaluated at ξ_m or ξ_p , must be interpolated from the surrounding nodal values. The currently employed interpolation algorithm utilizes a Lagrangian polynomial.

Together with the boundary conditions equations (B.4) through (B.6) constitute a system in the unknowns U_j^n , V_j^n , and F_j^n . Because of the nonlinear convection term Newton's method is adopted to linearize the equations. The linearized equations can be written in terms of the unknown corrections $\delta U_j^{i,n,\kappa}$, $\delta V_j^{i,n,\kappa}$, and $\delta F_j^{i,n,\kappa}$

$$-\frac{1}{r_i} (\delta U_j^{i,n,\kappa} + \delta U_{j-1}^{i,n,\kappa}) + \frac{1}{h_j} (\delta F_j^{i,n,\kappa} - \delta F_{j-1}^{i,n,\kappa}) = (r_1^C)_j^{i,n,\kappa} \quad (B.7)$$

$$(s_1^C)_j^{i,n,\kappa} \delta V_j^{i,n,\kappa} + (s_2^C)_j^{i,n,\kappa} \delta V_{j-1}^{i,n,\kappa} + (s_3^C)_j^{i,n,\kappa} \delta F_j^{i,n,\kappa} + (s_4^C)_j^{i,n,\kappa} \delta F_{j-1}^{i,n,\kappa} + (s_5^C)_j^{i,n,\kappa} \delta U_j^{i,n,\kappa} + (s_6^C)_j^{i,n,\kappa} \delta U_{j-1}^{i,n,\kappa} = (r_2^C)_j^{i,n,\kappa} \quad (B.8)$$

$$\delta U_j^{i,n,\kappa} - \delta U_{j-1}^{i,n,\kappa} - \frac{h_j}{2} (\delta V_j^{i,n,\kappa} + \delta V_{j-1}^{i,n,\kappa}) = -(U_j^{i,n,\kappa-1} - U_{j-1}^{i,n,\kappa-1}) + h_j V_{j-1/2}^{i,n,\kappa-1} \quad (B.9)$$

where the superscript κ denotes the iteration counter. The structure of the resulting system is identical to that of the regular box scheme, and the only change occurs in the coefficients, which now are defined by

$$\begin{aligned} (s_1^C)_j^{i,n,\kappa} &= \frac{b_j^{i,n}}{h_j} + \frac{1}{4} (F_{j-1/2}^{i,n,\kappa-1} + F_{j-1/2}^{m,n-1}) \\ (s_2^C)_j^{i,n,\kappa} &= -\frac{b_{j-1}^{i,n}}{h_j} + \frac{1}{4} (F_{j-1/2}^{i,n,\kappa-1} + F_{j-1/2}^{m,n-1}) \\ (s_3^C)_j^{i,n,\kappa} &= (s_4^C)_j^{i,n,\kappa} = \frac{1}{4} (V_{j-1/2}^{i,n,\kappa-1} + V_{j-1/2}^{m,n-1}) \\ (s_5^C)_j^{i,n,\kappa} &= -\frac{1}{k_n} - \frac{(U_{j-1/2}^{i,n,\kappa-1} - U_{j-1/2}^{m,n-1}) U_j^{i,n,\kappa-1}}{k_n \left[\sqrt{1 + (U^2)_{j-1/2}^{i,n,\kappa-1}} + \sqrt{1 + (U^2)_{j-1/2}^{m,n-1}} \right] \sqrt{1 + (U^2)_{j-1/2}^{i,n,\kappa-1}}} \\ (s_6^C)_j^{i,n,\kappa} &= -\frac{1}{k_n} - \frac{(U_{j-1/2}^{i,n,\kappa-1} - U_{j-1/2}^{m,n-1}) U_{j-1}^{i,n,\kappa-1}}{k_n \left[\sqrt{1 + (U^2)_{j-1/2}^{i,n,\kappa-1}} + \sqrt{1 + (U^2)_{j-1/2}^{m,n-1}} \right] \sqrt{1 + (U^2)_{j-1/2}^{i,n,\kappa-1}}} \\ (r_1^C)_j^{i,n,\kappa} &= -\frac{1}{h_j} (F_j^{i,n,\kappa-1} + F_j^{i-1,n} - F_{j-1}^{i,n,\kappa-1} - F_{j-1}^{i-1,n}) + \frac{2}{r_i} (U_{j-1/2}^{i,n,\kappa-1} - U_{j-1/2}^{i-1,n}) \\ (r_2^C)_j^{i,n,\kappa} &= -\left\{ \frac{b_j^{i,n} V_j^{i,n,\kappa-1} - b_{j-1}^{i,n} V_{j-1}^{i,n,\kappa-1}}{h_j} + \frac{(bV)_j^{m,n-1} - (bV)_{j-1}^{m,n-1}}{h_j} \right. \\ &\quad \left. + \frac{1}{2} (F_{j-1/2}^{i,n,\kappa-1} + F_{j-1/2}^{m,n-1}) (V_{j-1/2}^{i,n,\kappa-1} + V_{j-1/2}^{m,n-1}) - \frac{2}{k_n} (U_{j-1/2}^{i,n,\kappa-1} - U_{j-1/2}^{m,n-1}) \right\} \\ &\quad - 2 \frac{W_{j-1/2}^{p,n} - W_{j-1/2}^{p,n-1}}{k_n} - \frac{(W^{i,n} + W_{j-1/2}^{m,n-1})(W^{i,n-1/2} - W_{j-1/2}^{m,n-1/2})}{\xi_i - \xi_m} \end{aligned} \quad (B.10)$$

Since the resulting equations of the characteristic box scheme are of the same form as those for the regular box, the same algorithm can be employed to obtain a solution. The equations are arranged in the same manner as described in Appendix A in order to form a block-tridiagonal system, which is solved by Keller's block elimination method.

Appendix C. The upstream boundary conditions

As is well known a mathematically well posed problem requires that the governing differential equations be accompanied by appropriate initial and boundary conditions. This appendix describes the method which provides the upstream boundary conditions for the unsteady boundary layer equations. The proposed method consists of an iterative computation of the flow at the stagnation point, and the adjacent upper and lower surface points. For the computation of the flow at the stagnation point, the method adopts a modified characteristic box scheme. In the following we will first derive the difference equations for the modified characteristic box scheme, and we will then outline the proceeding how to obtain the upstream boundary conditions.

The modified characteristic box scheme differs from the original one in that the continuity and the momentum equations of the modified scheme are solved in a decoupled manner. Consequently, the tangential component u and the normal component v of the velocity are calculated separately, the first one by solving the momentum equation, the latter one by solving the continuity equation. It is this decoupling and the use of a characteristic box scheme, which allows the solution of the flow at the very first point on a new timeline. The difficulty of this endeavour lies in that there is absolutely no information available on the new timeline. This disables the regular box scheme, because it would involve a ξ -derivative on the new timeline (requiring a known point there). The solution of the continuity equation is impeded for the same reason. However, there is a drawback associated with the decoupled method, that is the normal velocity component v must be assumed known in the momentum equation. This entails an iterative procedure, which proceeds as follows. The first step of each of those iterations solves the momentum equation for a known, though provisional value of the normal velocity component v , which is taken from the previous level of iteration. Subsequently, the second step updates the normal velocity component v by solving the continuity equation. This procedure is repeated till successive values of the normal velocity component v differ by less than a prescribed small quantity.

We will now briefly present the equations for the modified characteristic box scheme. The system of first-order partial differential equations is reduced to two (since the continuity equation is left out), namely the momentum equation and the auxiliary equation, which results from the introduction of the new dependent variable V

$$\frac{\partial}{\partial \eta} (bV) + \tilde{F}V - \sqrt{1 + U^2} \frac{\partial U}{\partial s} = -\frac{\partial W}{\partial \tau} - W \frac{\partial W}{\partial \xi} \quad (C.1)$$

$$\frac{\partial U}{\partial \eta} - V = 0 \quad (C.2)$$

The tilde indicates provisional values that are taken from the previous level of iteration. Because F is treated as a known coefficient, there are only two boundary conditions necessary

$$\begin{aligned} \eta = 0: \quad U &= 0 \\ \eta = \eta_e: \quad U &= W(\xi, \tau) \end{aligned} \quad (C.3)$$

The discretization follows the previously outlined procedure, with the momentum equation being centered at the point $(\xi_p, \eta_{j-1/2}, \tau_{n-1/2})$, and the auxiliary equation at the point $(\xi_i, \eta_{j-1/2}, \tau_n)$. After employing Newton's linearization the system can be rewritten as

$$(s_1^D)_j^{i,n,\kappa} \delta V_j^{i,n,\kappa} + (s_2^D)_j^{i,n,\kappa} \delta V_{j-1}^{i,n,\kappa} + (s_3^D)_j^{i,n,\kappa} \delta U_j^{i,n,\kappa} + (s_4^D)_j^{i,n,\kappa} \delta U_{j-1}^{i,n,\kappa} = (r_1^D)_j^{i,n,\kappa} \quad (C.4)$$

ORIGINAL SOURCE OF
OF POOR QUALITY

$$\delta U_j^{i,n,\kappa} - \delta U_{j-1}^{i,n,\kappa} - \frac{h_j}{2} (\delta V_j^{i,n,\kappa} + \delta V_{j-1}^{i,n,\kappa}) = -(U_j^{i,n,\kappa-1} - U_{j-1}^{i,n,\kappa-1}) + h_j V_{j-1/2}^{i,n,\kappa-1} \quad (C.5)$$

where the coefficients $(s_k^D)_j^{i,n,\kappa}$ and $(r_1^D)_j^{i,n,\kappa}$ are defined by

$$\begin{aligned} (s_1^D)_j^{i,n,\kappa} &= \frac{b_j^{i,n}}{h_j} + \frac{1}{4} (\tilde{F}_{j-1/2}^{i,n} + F_{j-1/2}^{m,n-1}) \\ (s_2^D)_j^{i,n,\kappa} &= -\frac{b_{j-1}^{i,n}}{h_j} + \frac{1}{4} (\tilde{F}_{j-1/2}^{i,n} + F_{j-1/2}^{m,n-1}) \\ (s_3^D)_j^{i,n,\kappa} &= -\frac{1}{k_n} - \frac{(U_{j-1/2}^{i,n,\kappa-1} - U_{j-1/2}^{m,n-1}) U_j^{i,n,\kappa-1}}{k_n \left[\sqrt{1 + (U^2)_{j-1/2}^{i,n,\kappa-1}} + \sqrt{1 + (U^2)_{j-1/2}^{m,n-1}} \right] \sqrt{1 + (U^2)_{j-1/2}^{i,n,\kappa-1}}} \\ (s_4^D)_j^{i,n,\kappa} &= -\frac{1}{k_n} - \frac{(U_{j-1/2}^{i,n,\kappa-1} - U_{j-1/2}^{m,n-1}) U_{j-1}^{i,n,\kappa-1}}{k_n \left[\sqrt{1 + (U^2)_{j-1/2}^{i,n,\kappa-1}} + \sqrt{1 + (U^2)_{j-1/2}^{m,n-1}} \right] \sqrt{1 + (U^2)_{j-1/2}^{i,n,\kappa-1}}} \\ (r_1^D)_j^{i,n,\kappa} &= -\left\{ \frac{b_j^{i,n} V_j^{i,n,\kappa-1} - b_{j-1}^{i,n} V_{j-1}^{i,n,\kappa-1}}{h_j} + \frac{(bV)_j^{m,n-1} - (bV)_{j-1}^{m,n-1}}{h_j} \right. \\ &\quad \left. + \frac{1}{2} (\tilde{F}_{j-1/2}^{i,n} + F_{j-1/2}^{m,n-1}) (V_{j-1/2}^{i,n,\kappa-1} + V_{j-1/2}^{m,n-1}) - \frac{2}{k_n} (U_{j-1/2}^{i,n,\kappa-1} - U_{j-1/2}^{m,n-1}) \right\} \\ &\quad - 2 \frac{W_{j-1/2}^{p,n} - W_{j-1/2}^{m,n-1}}{k_n} - \frac{(W^{i,n} + W_{j-1/2}^{m,n-1})(W^{i,n-1/2} - W_{j-1/2}^{m,n-1/2})}{\xi_i - \xi_m} \end{aligned} \quad (C.6)$$

Together with the boundary conditions equations (C.4) and (C.5) form a system of $2J$ algebraically linear equations (where J is the number of gridpoints across the boundary layer). After proper arrangement of the equations, the resulting block tridiagonal system can be solved by the block elimination method, which has here to operate on 2×2 blocks.

We will finally turn to the procedure of obtaining the upstream boundary conditions. The flow at the stagnation point, which represents the upstream boundary conditions for both upper and lower surface, is obtained by an iterative procedure, in which each sweep involves the solution for the flow at the stagnation point and at the adjacent upper and lower surface points. In detail the procedure consists of the following steps:

1. For the initial iteration F must be guessed at the stagnation point. For that purpose F is linearly extrapolated on basis of the two preceding timelines

$$[\tilde{F}_j^{i,n}]^0 = F_j^{i,n-1} + \frac{k_n}{k_{n-1}} (F_j^{i,n-1} - F_j^{i,n-2}) \quad (C.7)$$

The superscript outside the brackets refers to the number of the sweep, the 0 in the above equation denotes the initial sweep.

2. The flow at the stagnation point is solved by means of the modified characteristic box scheme. The results U and V are of approximate nature, since F is assumed known from the previous level of iteration.
3. The flow at the adjacent upper surface point is solved by the usual procedure. That is the regular box scheme is used for that part of the boundary layer, where the tangential

velocity component is directed downstream, while the characteristic box scheme is employed in regions of backflow.

4. The flow at the adjacent lower surface point is solved by the same procedure that is used for the upper surface point.
5. The provisional values of F are updated by utilizing the (so-far unused) continuity equation

$$[\tilde{F}_j^{i,n}]^\lambda = [\tilde{F}_{j-1}^{i,n}]^\lambda + \frac{h_j}{2} \left[\left(\frac{\partial U}{\partial \xi} \right)_{j,n}^{i,n} + \left(\frac{\partial U}{\partial \xi} \right)_{j-1,n}^{i,n} \right] \quad (C.8)$$

subject to the boundary condition (of zero normal velocity at the wall)

$$[\tilde{F}_1^{i,n}]^\lambda = 0 \quad (C.9)$$

The ξ - derivatives in equation (C.8) are approximated by means of Lagrangian polynomials, which are based upon the values at the stagnation point (index i), the upper surface point (index $i + 1$), and the lower surface point (index $i - 1$)

$$\begin{aligned} \left(\frac{\partial U}{\partial \xi} \right)_{j,n}^{i,n} = & U_j^{i-1,n} \frac{(\xi_i - \xi_{i+1})}{(\xi_{i-1} - \xi_i)(\xi_{i-1} - \xi_{i+1})} + U_j^{i,n} \frac{(2\xi_i - \xi_{i-1} - \xi_{i+1})}{(\xi_i - \xi_{i-1})(\xi_i - \xi_{i+1})} \\ & + U_j^{i+1,n} \frac{(\xi_i - \xi_{i-1})}{(\xi_{i+1} - \xi_{i-1})(\xi_{i+1} - \xi_i)} \end{aligned} \quad (C.10)$$

6. Finally it is checked, whether the values of F have converged to a prescribed accuracy. If successive values of F at the boundary layer edge differ by less than a given tolerance, then the procedure is exited and a set of upstream boundary conditions has been established. Else the procedure continues with the second step and is repeated till the criterion of convergence is met.

Appendix D. Guesses for the initial Newton iteration

The solution of the nonlinear boundary layer equations requires that the equations be linearized by Newton's method. In this method the dependent variables are substituted by the (known) variables of the previous level of iteration plus a small correction. After dropping the quadratic terms, the equations are solved for the unknown corrections. In order to start the iteration an initial guess of the dependent variables must be provided. The quality of this initial guess has a great deal of influence on the number of the required iterations, and ultimately, a bad guess can lead to diverging results. A simple, though inaccurate guess would be given by the values of either the adjacent upstream station or the previous timeline. In our code the initial guess for U is obtained from a two-step procedure, which consists of an extrapolation and an adjustment to the imposed external velocity. The extrapolation is preferably performed in time, since the results of two succeeding timelines are usually closer than those of two adjacent streamwise stations. The velocity profile obtained from the extrapolation is adjusted to the given external velocity in order to automatically satisfy the boundary condition at the boundary layer edge. Guesses for the remaining two variables V and F follow from the solution of the auxiliary and the continuity equations with the guessed U profile as input.

If possible we base our scheme on a linear extrapolation of U in time and a proportional adjustment of the extrapolated profile (designated by a caret) to the external velocity

$$\begin{aligned}\hat{U}_j^{i,n,0} &= U_j^{i,n-1} + \frac{\tau_n - \tau_{n-1}}{\tau_{n-1} - \tau_{n-2}} (U_j^{i,n-1} - U_j^{i,n-2}) \\ U_j^{i,n,0} &= \hat{U}_j^{i,n,0} \frac{W^{i,n}}{\hat{U}_j^{i,n,0}}\end{aligned}\quad (D.1)$$

This extrapolation scheme can only be employed, if both $W^{i,n}$ and $\hat{U}_j^{i,n,0}$ do not equal zero. In case one of these conditions is violated, we adopt a slightly modified scheme. There the adjustment to the external velocity is achieved by the choice of a proper $\partial U / \partial \tau$

$$U_j^{i,n,0} = U_j^{i,n-1} + \frac{W^{i,n} - W^{i,n-1}}{W^{i,n-1} - W^{i,n-2}} (U_j^{i,n-1} - U_j^{i,n-2}) \quad (D.2)$$

This scheme requires that both terms $(W^{i,n} - W^{i,n-1})$ and $(W^{i,n-1} - W^{i,n-2})$ be nonzero. If both procedures fail, we combine the first step of the first procedure with a single adjustment of the outermost point to the given external velocity.

The values of V can be guessed by differentiating the above obtained U

$$\begin{aligned}V_j^{i,n,0} &= -V_{j+1}^{i,n,0} + \frac{2}{h_{j+1}} (U_{j+1}^{i,n,0} - U_j^{i,n,0}) \\ V_j^{i,n,0} &= 0\end{aligned}\quad (D.3)$$

An estimation of F is obtained from the substitution of the guessed U into the continuity equation (subject to the condition of zero normal velocity at the wall)

$$\begin{aligned}F_j^{i,n,0} &= F_{j-1}^{i,n,0} - (F_j^{i-1,n} - F_{j-1}^{i-1,n}) + \frac{2h_j}{r_i} (U_{j-1/2}^{i,n,0} - U_{j-1/2}^{i-1,n}) \\ F_1^{i,n,0} &= 0\end{aligned}\quad (D.4)$$

Appendix E. On instabilities of the near-wall solutions

The standard box method, as devised by Keller and Cebeci, allows the occurrence of streamwise oscillations in the near-wall solutions of the boundary layer. The oscillations are caused by the centered discretization of the momentum equation, which, by taking two-point averages, may offset the errors of symmetrically overshooting solutions at the upstream and the downstream faces of the difference molecule. Similar observations were made by Drela and Thompkins /17,18/ in their study of non-unique solutions of boundary layer equations. Though the possible occurrence of these oscillations is, according to our experience, an inherent shortcoming of the box method, Cebeci never reported on problems of this kind. This might be related to the fact that a well-smoothed external velocity distribution (as input) and the use of a well-adapted boundary layer grid do suppress the oscillations to a great extent. As a matter of fact, we only became aware of the problem, when we tried to run a steady flow case in physical coordinates. In the following we will give the reason for the occurrence of overshooting solutions, and briefly describe our proposed modification to the box scheme in order to ensure a smooth solution.

For the sake of simplicity we shall explain the development of these instabilities for the steady, laminar boundary layer. The momentum equation reduces then at the wall to

$$v \frac{\partial^2 u}{\partial y^2} \cong -u_e \frac{\partial u_e}{\partial x} \quad (E.1)$$

This equation retains only the viscous and the pressure terms, and is exact at $y = 0$. Further, the equation approximately holds true in the near-wall field, where those two terms dominate the balance of momentum. The box method requires the momentum equation be discretized at the center of the box such that equation (E.1) is approximated by

$$\frac{v}{2} \left[\left(\frac{\partial^2 u}{\partial y^2} \right)^i + \left(\frac{\partial^2 u}{\partial y^2} \right)^{i-1} \right] \cong - \left(u_e \frac{\partial u_e}{\partial x} \right)^{i-1/2} \quad (E.2)$$

Since this equation only deals with the average of $\partial^2 u / \partial y^2$ between two successive streamwise stations, $\partial^2 u / \partial y^2$, and consequently u , may exhibit oscillatory deviations and still satisfy the equation. The error at the i th station is simply compensated by an equal error of opposite sign at the $i-1$ st station. Unfortunately, at the wall there is no mechanism to dampen these oscillations, whereas there is one further away from the wall. With the convective terms gaining weight in the momentum balance, the profile of u is increasingly constrained by the need to approach the prescribed, external velocity. Finally there remains the question, how the oscillations get started. Two causes are believed to initiate the first deviation from a smooth solution: First, a slightly uneven external velocity distribution, as was demonstrated by Drela with his zero-pressure gradient flow responding to a 5 percent jump of the edge velocity, and second, the sudden change of flow conditions at successive streamwise stations on $\eta = \text{constant}$ lines, as possible in poorly adaptive grids that do not account for the growth of the boundary layer. Before we proceed with our proposed modification of the box scheme, we would like to point out again that these instabilities do only occur near the wall, and they have not been observed for the standard, steady scheme with the use of transformed coordinates (at least the amplitudes of the oscillations there are reduced to a negligible degree).

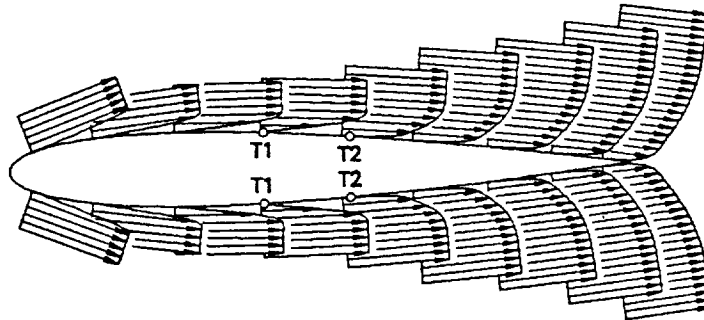
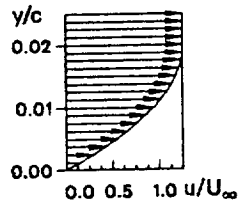
The oscillations are numerically only possible, because the point, where the boundary layer equations are satisfied, is separate from the point, where the solution is actually computed.

Based on this finding the box method was modified in that the solution is now taken at that point, which actually satisfies the equations, which is the center of the box. The box method still solves for the variables at the downstream face of the difference molecule, but the variables, which are given as the solution, and which are used in the further calculations, are those associated with the center of the difference molecule. These variables are the two-point averages of the upstream and the downstream faces of the difference molecule in case of steady flow, or the four-point averages of the upstream and the downstream, as well as the current and the previous timeline nodes in case of unsteady flow. Though this procedure completely eliminates the occurrence of streamwise oscillations in the near-wall solutions, it may be a mixed blessing. While the modified scheme formally retains second order accuracy, the actual truncation error might become larger due to the implicit smoothing. Furthermore, under the assumption of the same meshsize in the streamwise direction, the required computational effort will double. In view of the shortcomings of both methods, one might well ventilate the question, whether a non-centered scheme will do a better job. Non-centered schemes will not experience instabilities of the above described kind, but in order to maintain second order accuracy, the streamwise derivatives must be approximated by one-sided, three-point difference representations. Veldman /45/ and his collaborators /23/ have made extensive use of the non-centered Crank-Nicolson method, and in view of their success a consideration of such a scheme might well be worthwhile.

BOUNDARY LAYER VELOCITY PROFILES

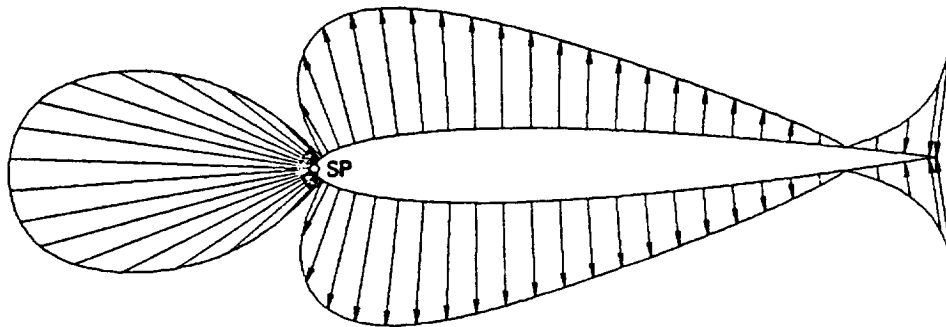
Symbols: T1 ... Begin of Transition
T2 ... End of Transition

B.L. SCALES

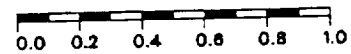


POTENTIAL FLOW PRESSURE DISTRIBUTION

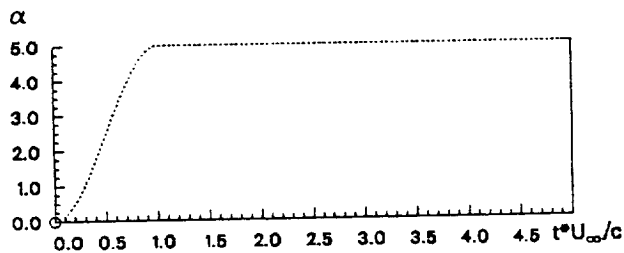
Symbols: SP ... Stagnation Point



PRESSURE SCALE



TIME HISTORY OF THE ANGLE OF ATTACK



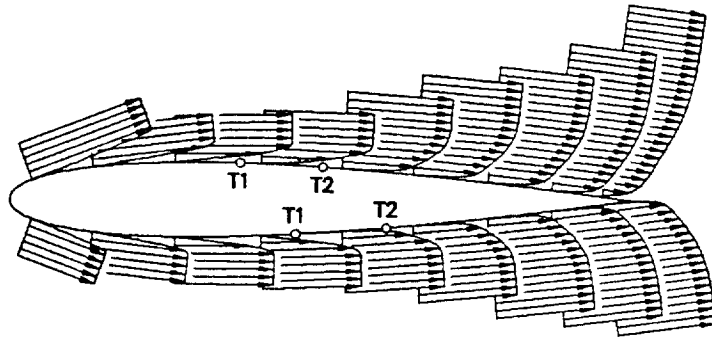
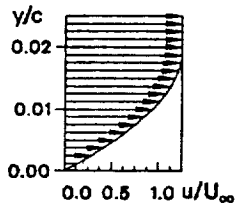
NACA 0012		87-11-10
Reynolds No:	1 mill,	BI Stations: 181
Trans Const:	120.,	Timesteps: 200
RAMP CHANGE IN AOA		
Initial AoA:	0deg,	Pivot: (0.00,0.0)
Final AoA:	5deg,	Rise Time: 1.00

Figure 1. The boundary layer velocity profiles and the pressure distributions of a NACA 0012, undergoing a ramp-change in angle of attack.

BOUNDARY LAYER VELOCITY PROFILES

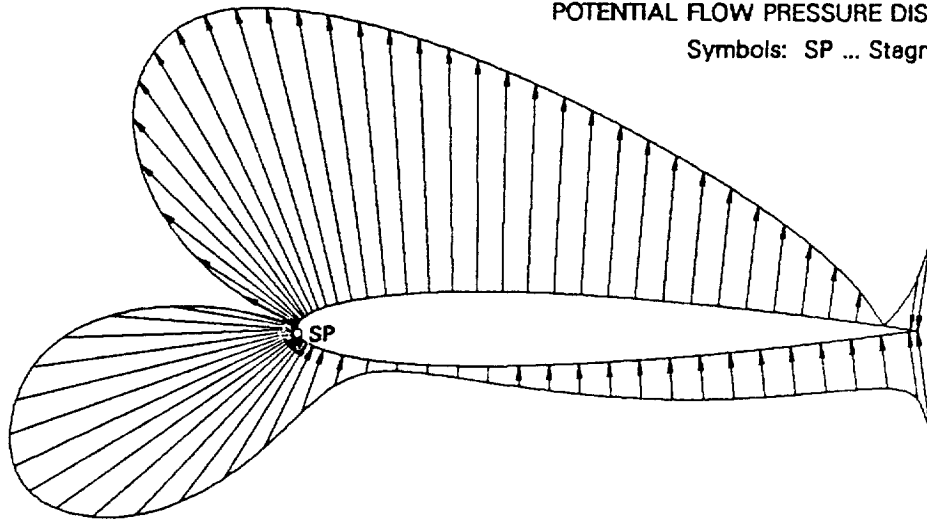
Symbols: T1 ... Begin of Transition
 T2 ... End of Transition

B.L. SCALES

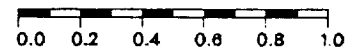


POTENTIAL FLOW PRESSURE DISTRIBUTION

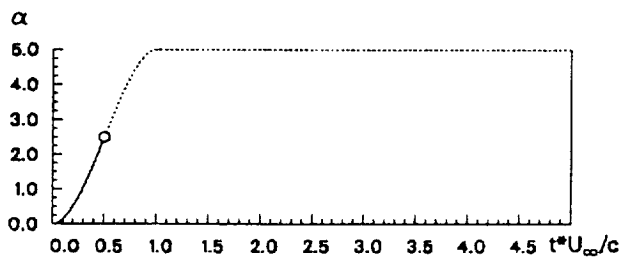
Symbols: SP ... Stagnation Point



PRESSURE SCALE



TIME HISTORY OF THE ANGLE OF ATTACK



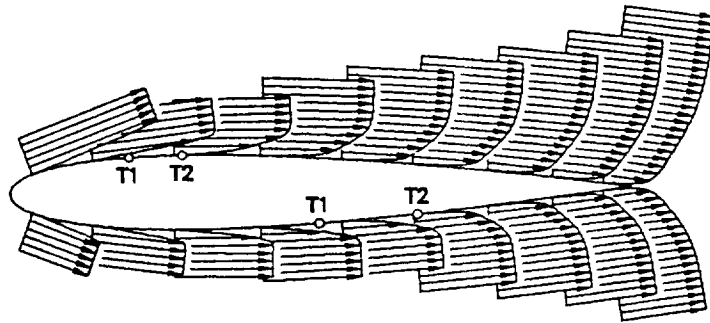
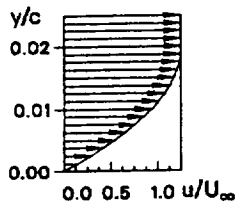
NACA 0012		87-11-10	
Reynolds No:	1 mill,	BI Stations:	181
Trans Const:	120.,	Timesteps:	200
RAMP CHANGE IN AOA			
Initial AoA:	0deg,	Pivot:	(0.00,0.0)
Final AoA:	5deg,	Rise Time:	1.00

Figure 1. (continued)

BOUNDARY LAYER VELOCITY PROFILES

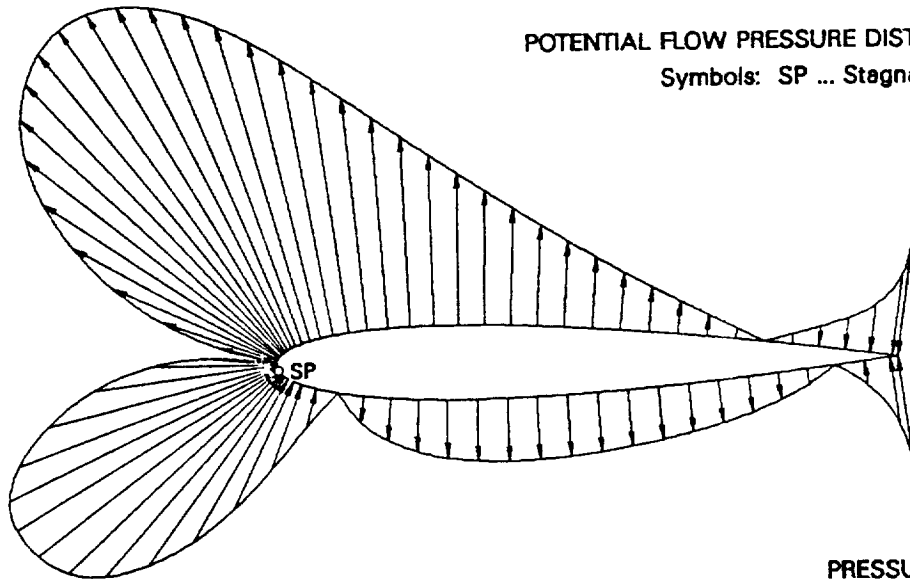
Symbols: T1 ... Begin of Transition
 T2 ... End of Transition

B.L. SCALES



POTENTIAL FLOW PRESSURE DISTRIBUTION

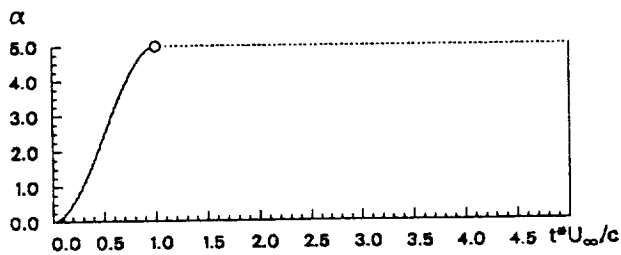
Symbols: SP ... Stagnation Point



PRESSURE SCALE



TIME HISTORY OF THE ANGLE OF ATTACK



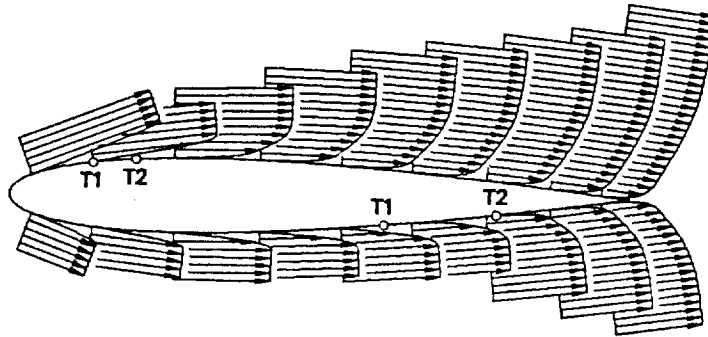
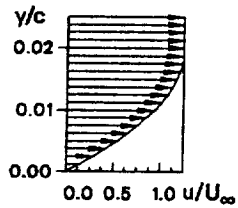
NACA 0012	87-11-10
Reynolds No: 1 mill,	BI Stations: 181
Trans Const: 120,	Timesteps: 200
RAMP CHANGE IN AOA	
Initial AoA: 0deg,	Pivot: (0.00,0.0)
Final AoA: 5deg,	Rise Time: 1.00

Figure 1. (continued)

BOUNDARY LAYER VELOCITY PROFILES

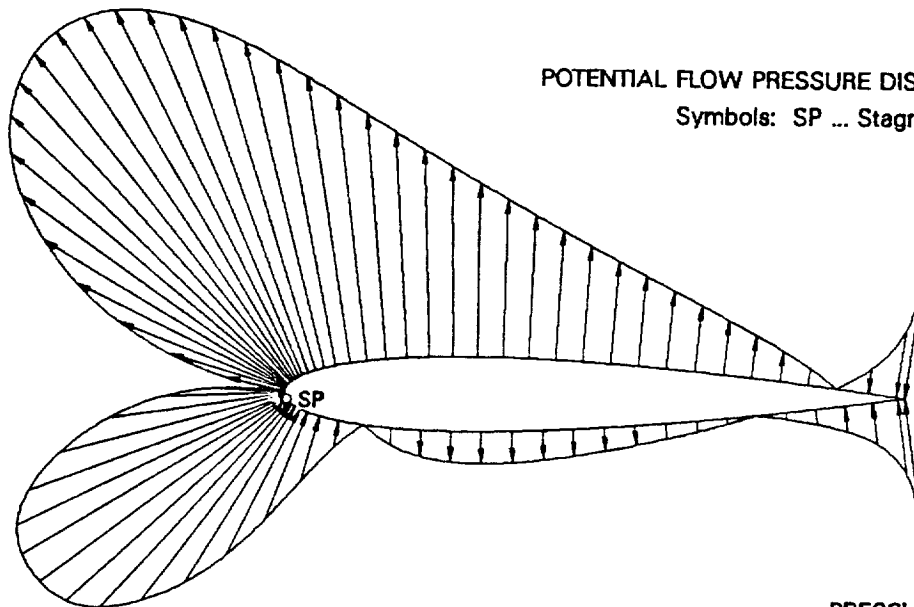
Symbols: T1 ... Begin of Transition
 T2 ... End of Transition

B.L. SCALES

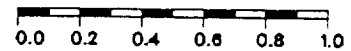


POTENTIAL FLOW PRESSURE DISTRIBUTION

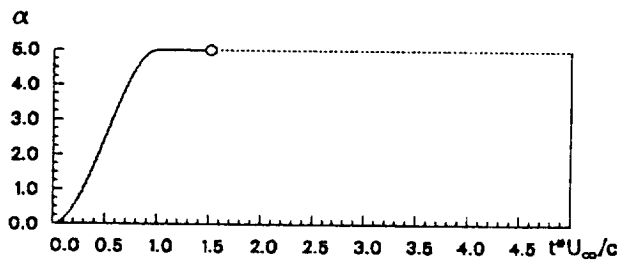
Symbols: SP ... Stagnation Point



PRESSURE SCALE



TIME HISTORY OF THE ANGLE OF ATTACK



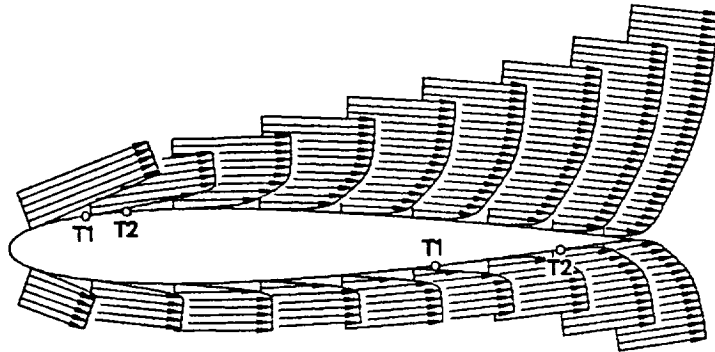
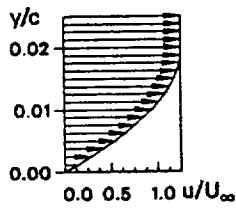
NACA 0012		87-11-10	
Reynolds No:	1 mill,	BI Stations:	181
Trans Const:	120.,	Timesteps:	200
RAMP CHANGE IN AOA			
Initial AoA:	0deg,	Pivot:	(0.00,0.0)
Final AoA:	5deg,	Rise Time:	1.00

Figure 1. (continued)

BOUNDARY LAYER VELOCITY PROFILES

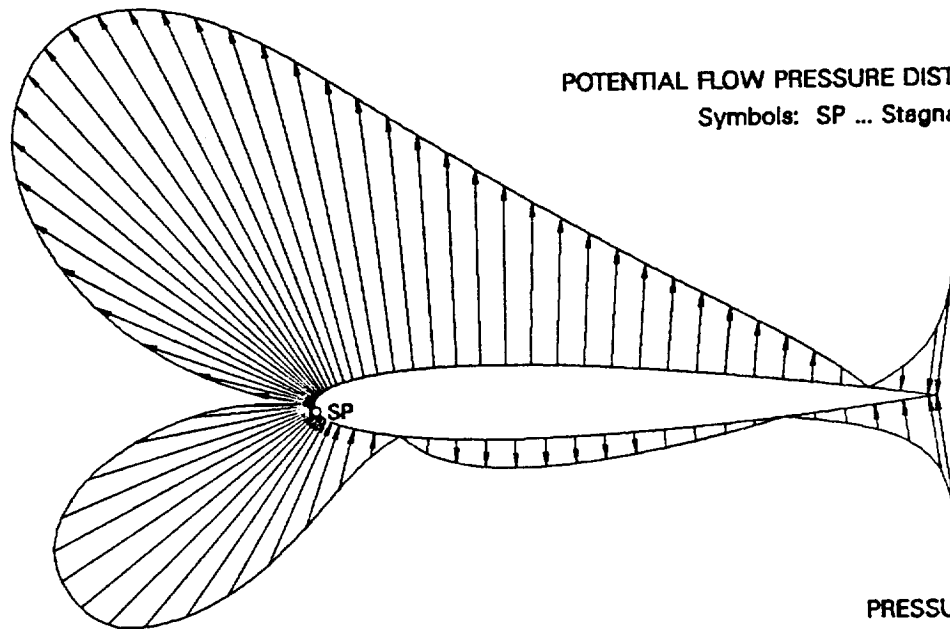
Symbols: T1 ... Begin of Transition
T2 ... End of Transition

B.L. SCALES



POTENTIAL FLOW PRESSURE DISTRIBUTION

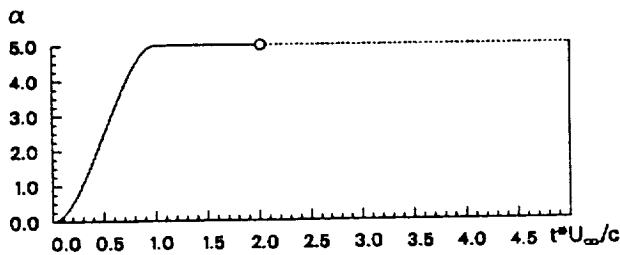
Symbols: SP ... Stagnation Point



PRESSURE SCALE



TIME HISTORY OF THE ANGLE OF ATTACK

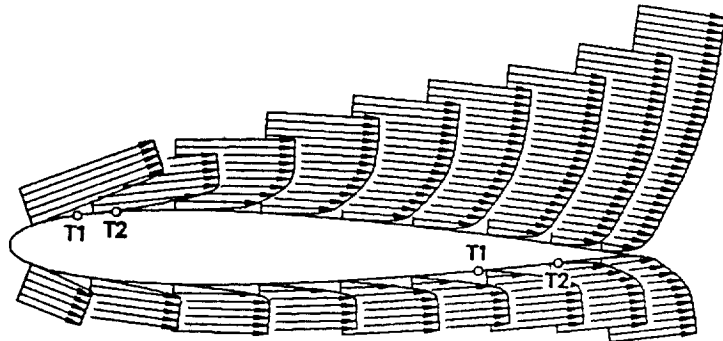
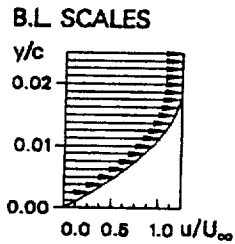


NACA 0012		87-11-10	
Reynolds No:	1 mill,	BI Stations:	181
Trans Const:	120.,	Timesteps:	200
RAMP CHANGE IN AOA			
Initial AoA:	0deg,	Pivot:	(0.00,0.0)
Final AoA:	5deg,	Rise Time:	1.00

Figure 1. (continued)

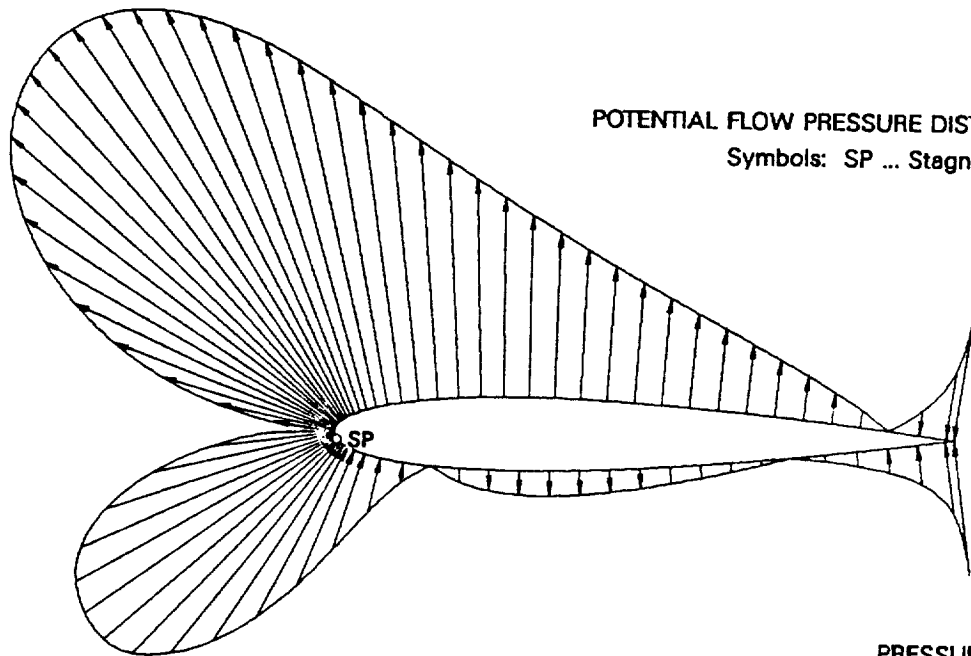
BOUNDARY LAYER VELOCITY PROFILES

Symbols: T1 ... Begin of Transition
T2 ... End of Transition

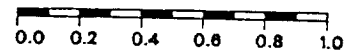


POTENTIAL FLOW PRESSURE DISTRIBUTION

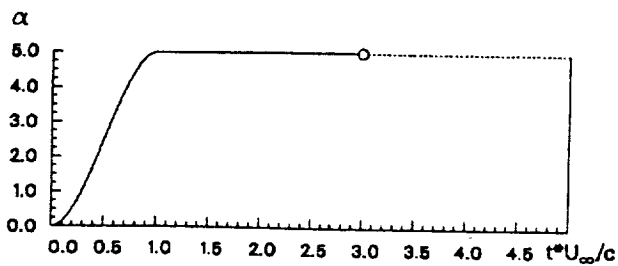
Symbols: SP ... Stagnation Point



PRESSURE SCALE



TIME HISTORY OF THE ANGLE OF ATTACK



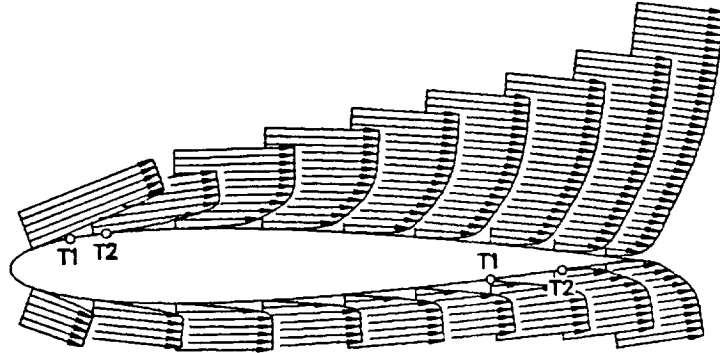
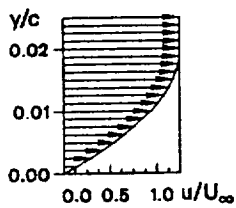
NACA 0012	87-11-10
Reynolds No: 1 mill,	BI Stations: 181
Trans Const: 120.,	Timesteps: 200
RAMP CHANGE IN AOA	
Initial AoA: 0deg,	Pivot: (0.00,0.0)
Final AoA: 5deg,	Rise Time: 1.00

Figure 1. (continued)

BOUNDARY LAYER VELOCITY PROFILES

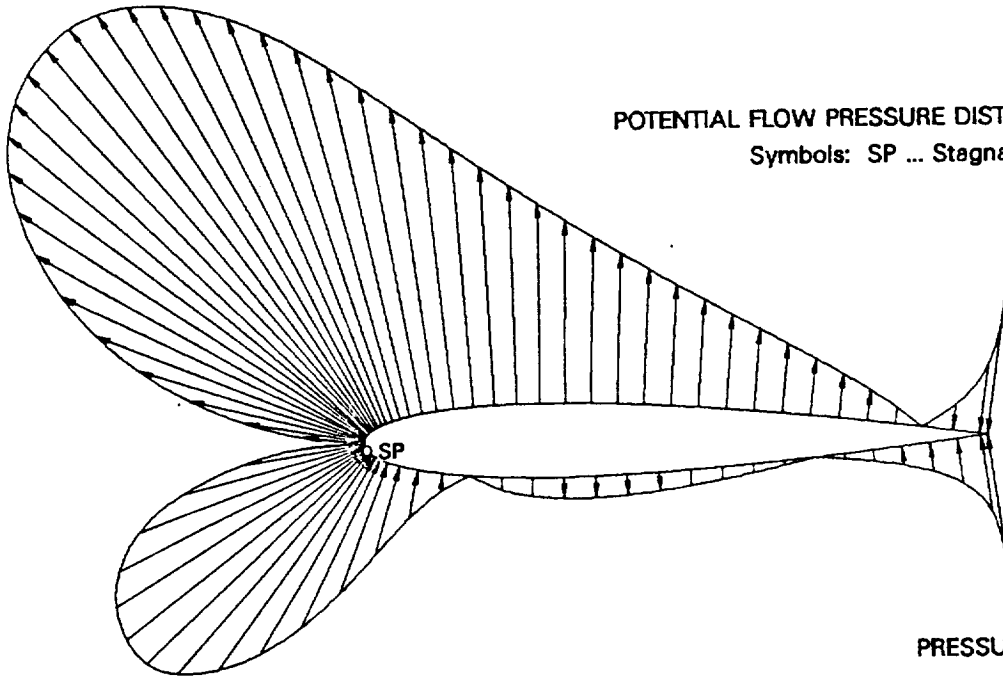
Symbols: T1 ... Begin of Transition
T2 ... End of Transition

B.L. SCALES



POTENTIAL FLOW PRESSURE DISTRIBUTION

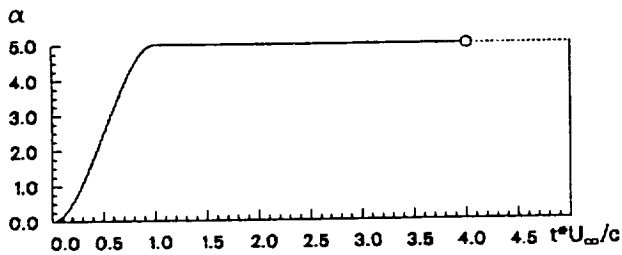
Symbols: SP ... Stagnation Point



PRESSURE SCALE



TIME HISTORY OF THE ANGLE OF ATTACK



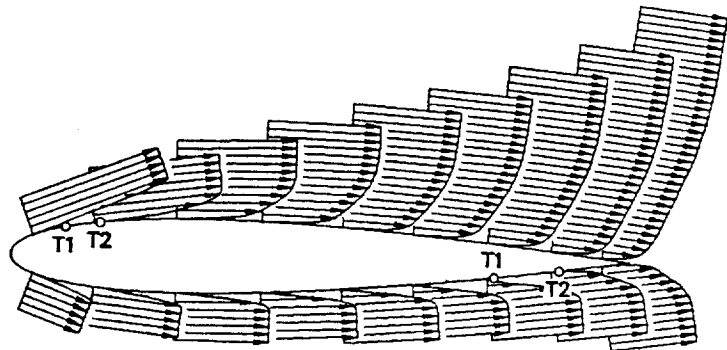
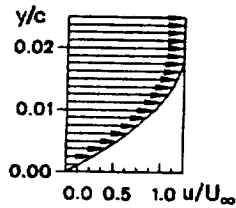
NACA 0012	87-11-10
Reynolds No: 1 mill,	BI Stations: 181
Trans Const: 120.,	Timesteps: 200
RAMP CHANGE IN AOA	
Initial AoA: 0deg,	Pivot: (0.00,0.0)
Final AoA: 5deg,	Rise Time: 1.00

Figure 1. (continued)

BOUNDARY LAYER VELOCITY PROFILES

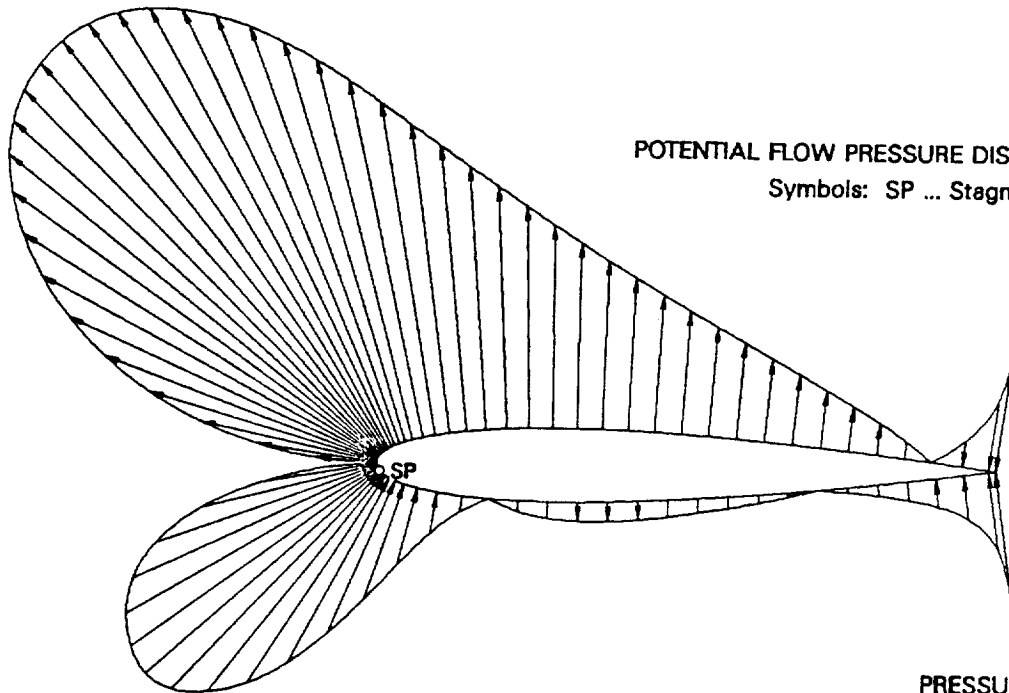
Symbols: T1 ... Begin of Transition
T2 ... End of Transition

B.L. SCALES

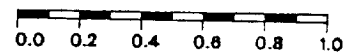


POTENTIAL FLOW PRESSURE DISTRIBUTION

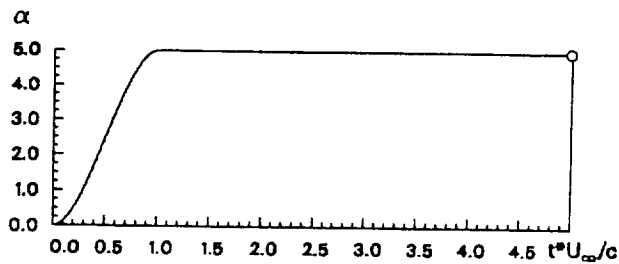
Symbols: SP ... Stagnation Point



PRESSURE SCALE



TIME HISTORY OF THE ANGLE OF ATTACK



NACA 0012	87-11-10
Reynolds No: 1 mill,	BI Stations: 181
Trans Const: 120.,	Timesteps: 200
RAMP CHANGE IN AOA	
Initial AoA: 0deg,	Pivot: (0.00,0.0)
Final AoA: 5deg,	Rise Time: 1.00

Figure 1. (continued)

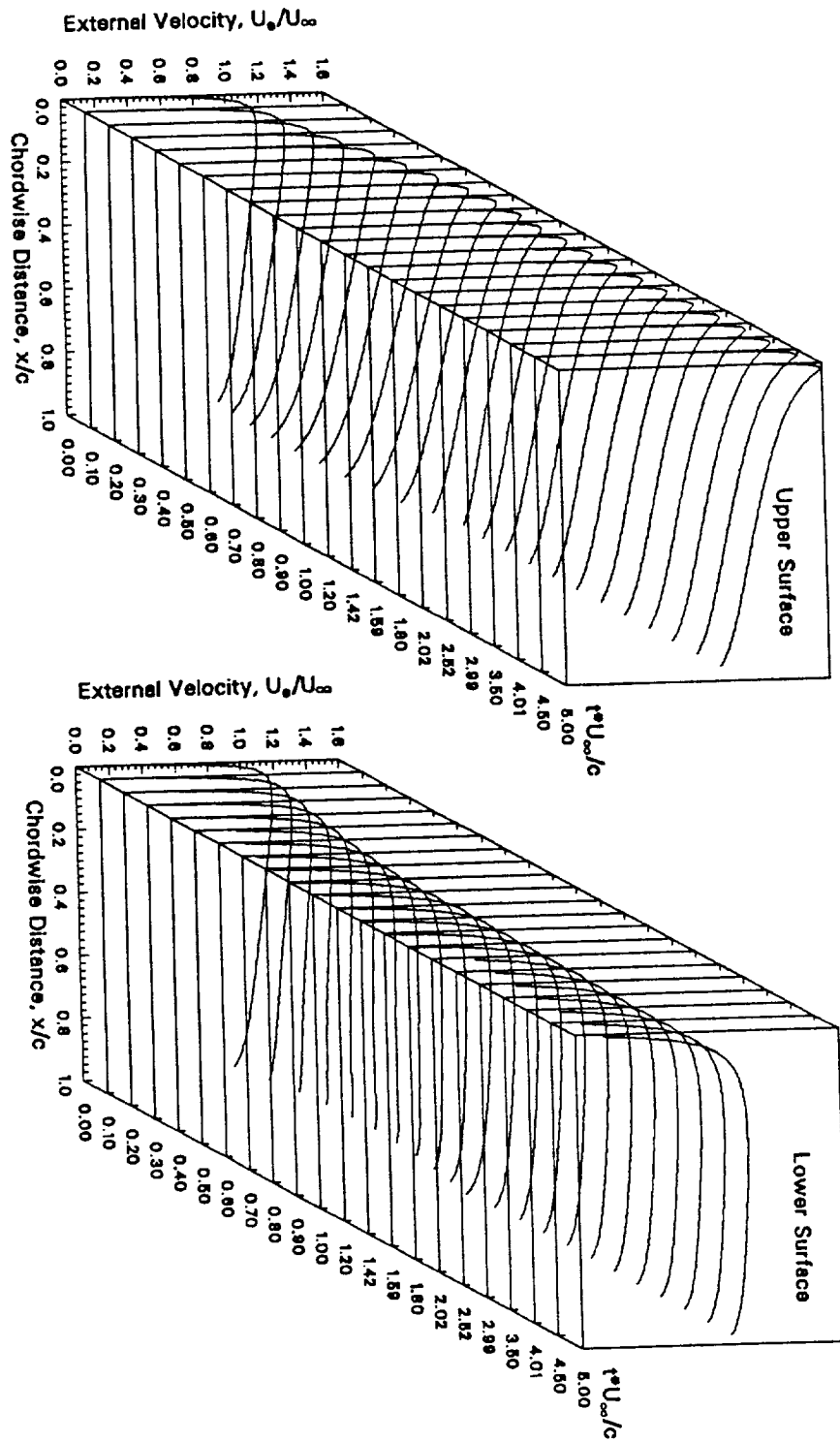


Figure 2. The external velocity distributions of a NACA 0012, undergoing a ramp-change in angle of attack.

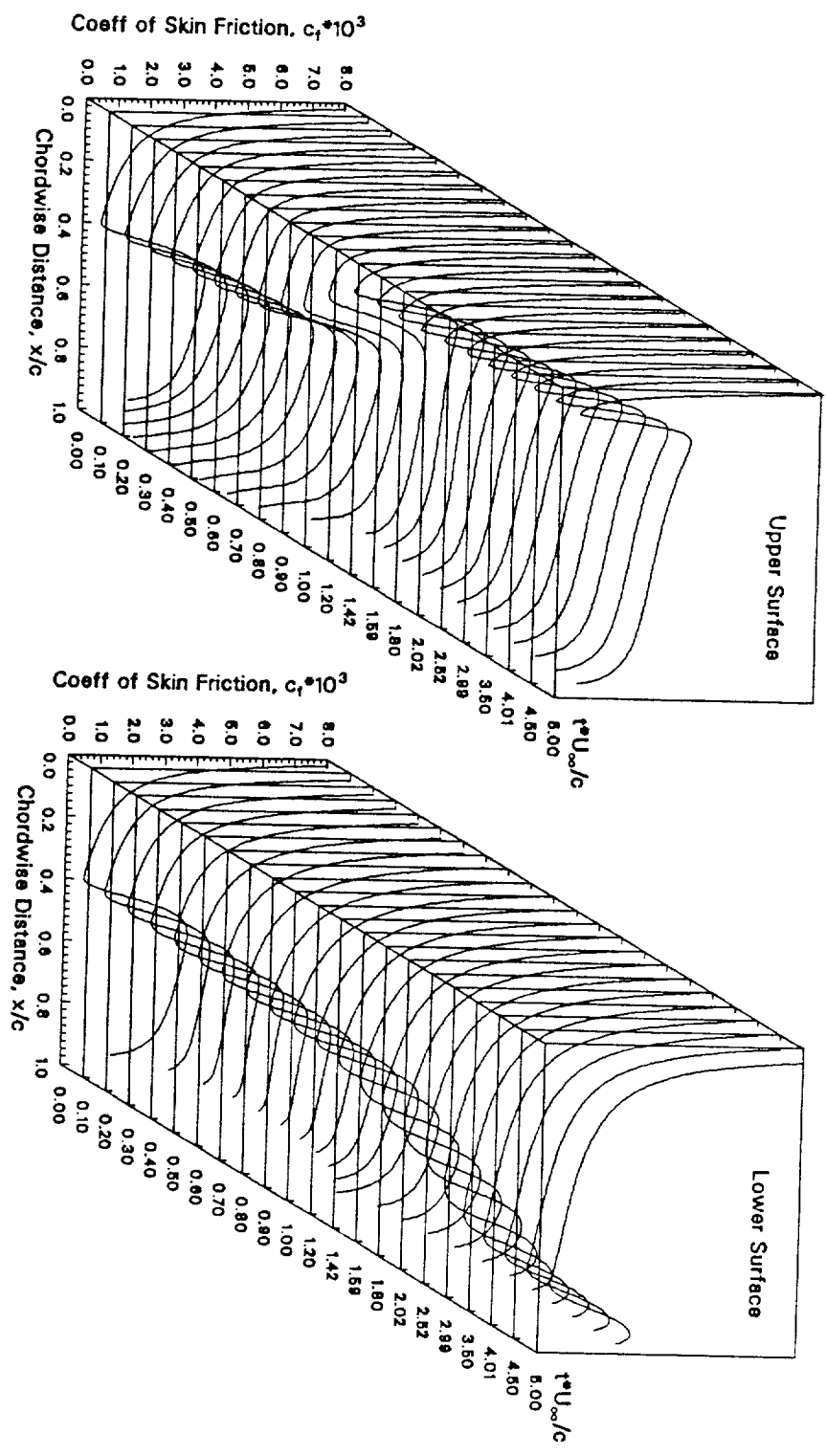


Figure 3. The distributions of skin friction of a NACA 0012, undergoing a ramp-change in angle of attack.

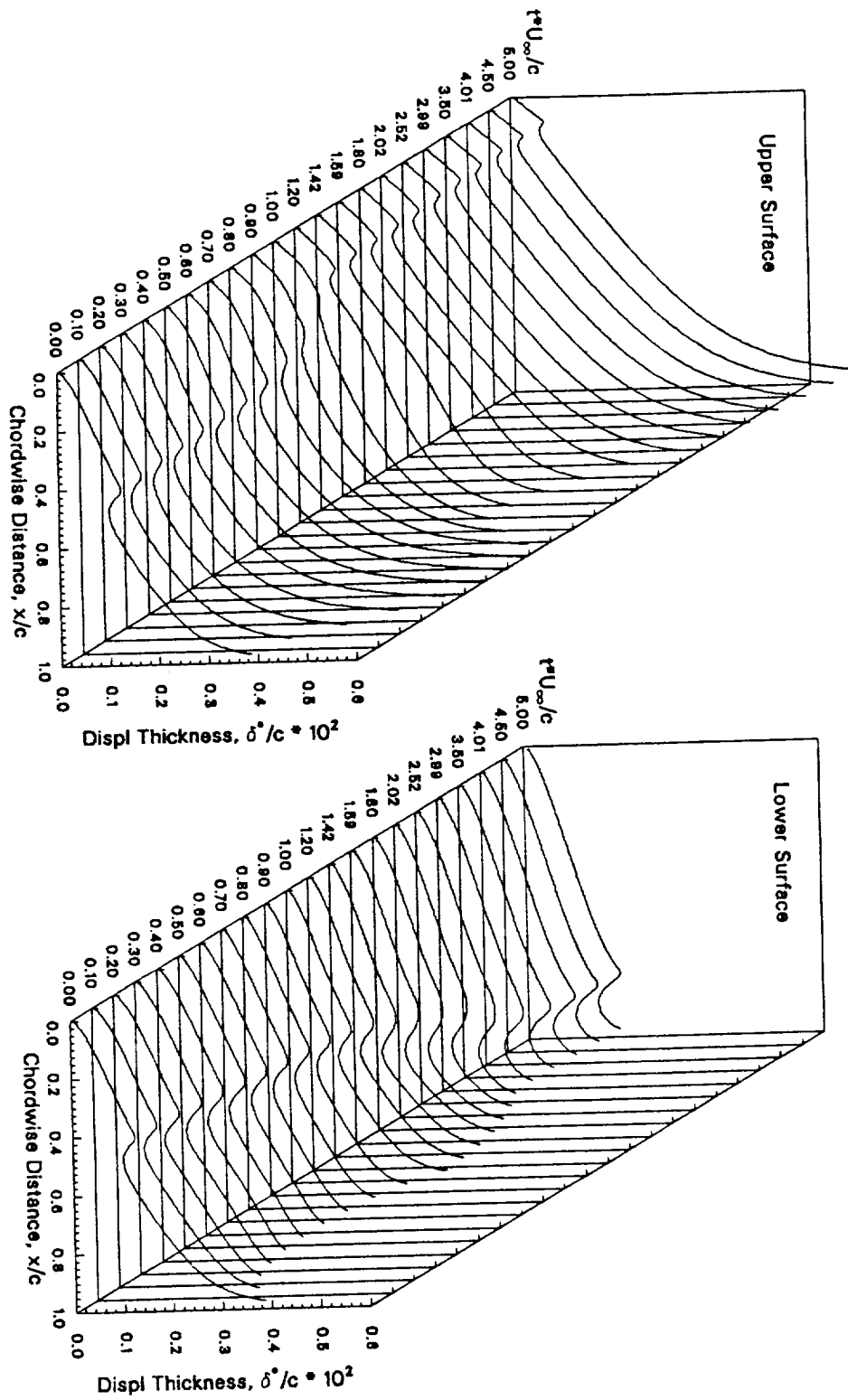


Figure 4. The distributions of displacement thickness of a NACA 0012, undergoing a ramp-change in angle of attack.

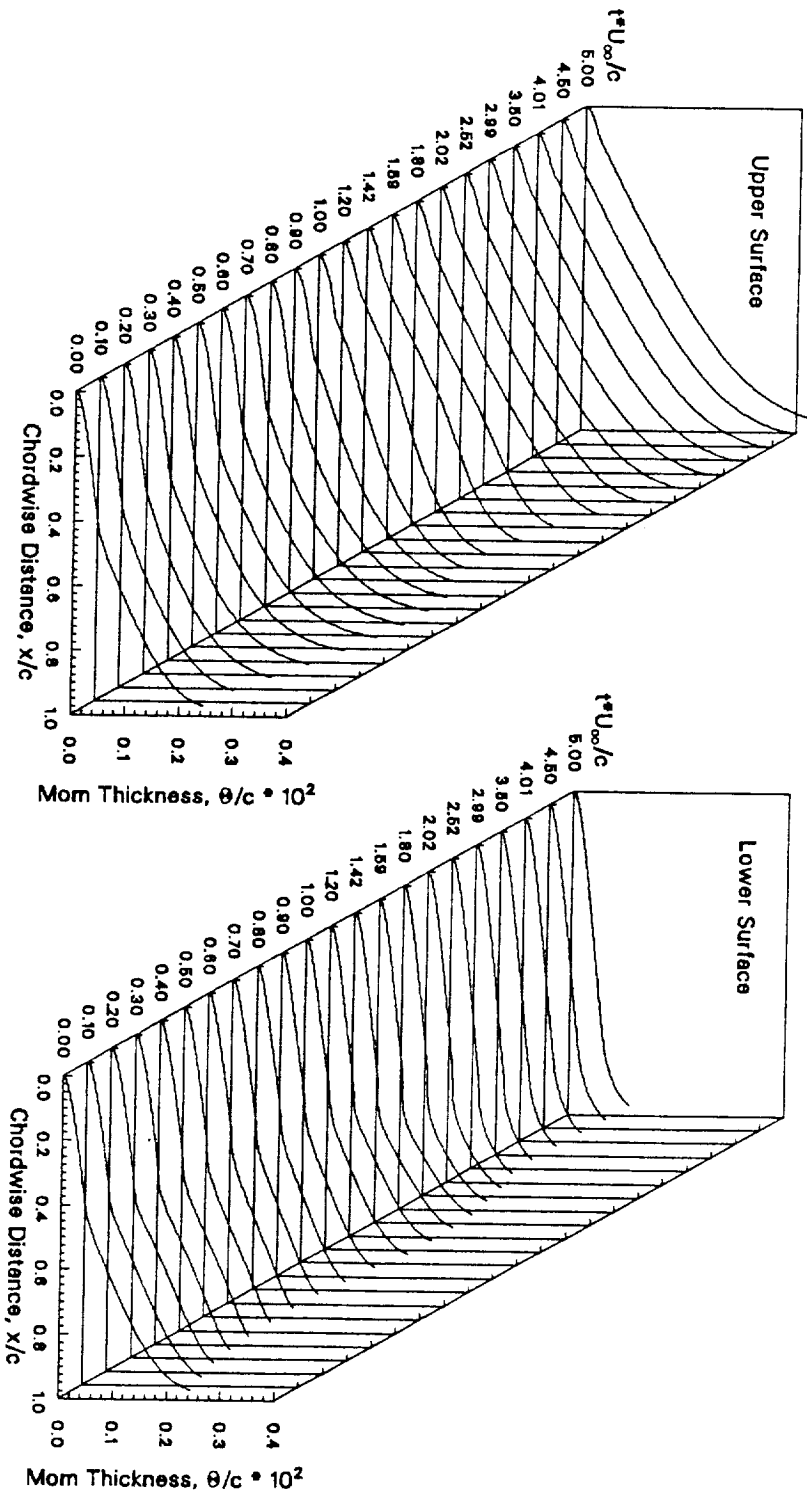


Figure 5. The distributions of momentum thickness of a NACA 0012, undergoing a ramp-change in angle of attack.

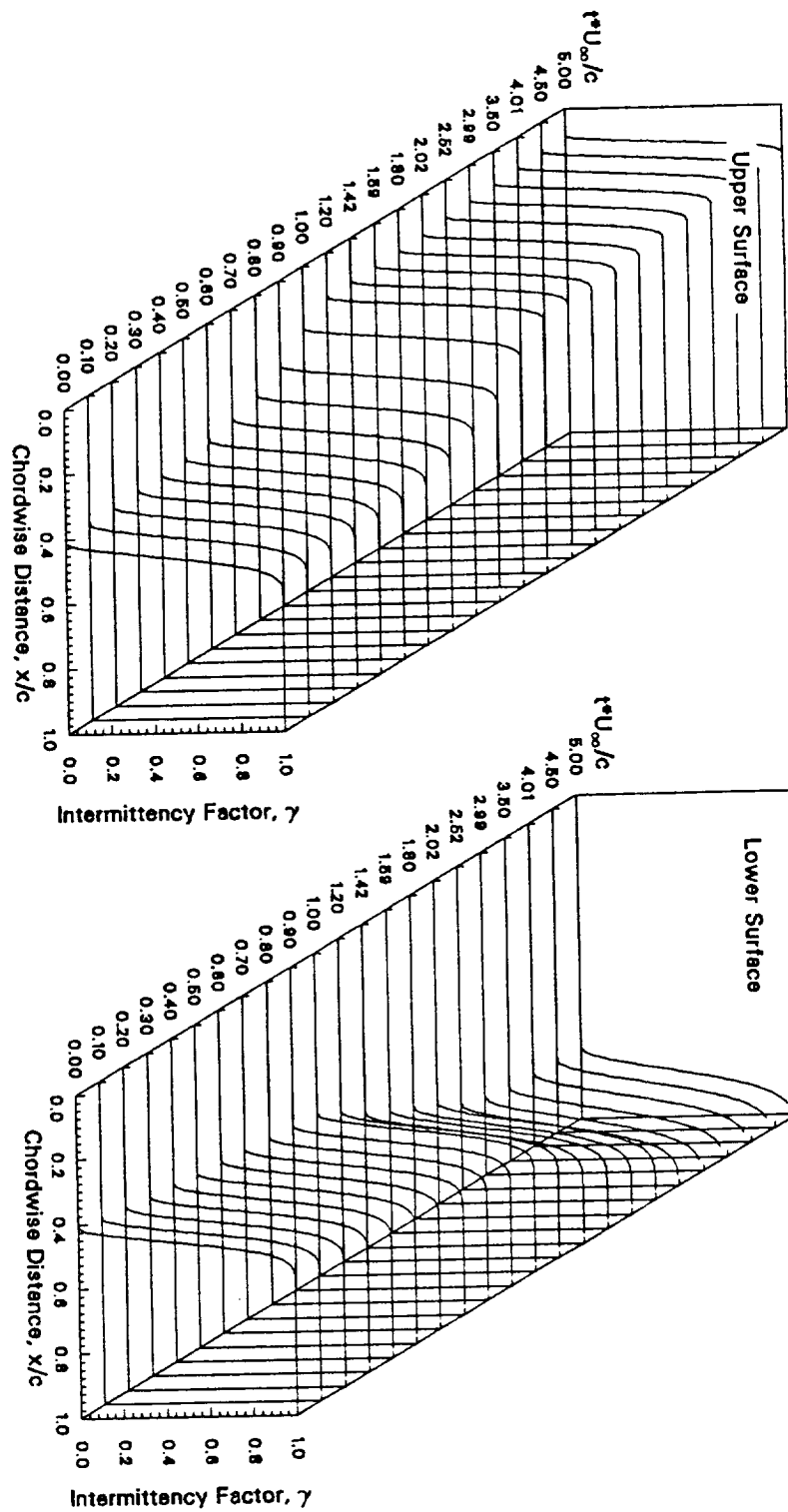


Figure 6. The distributions of intermittency of a NACA 0012, undergoing a ramp-change in angle of attack.

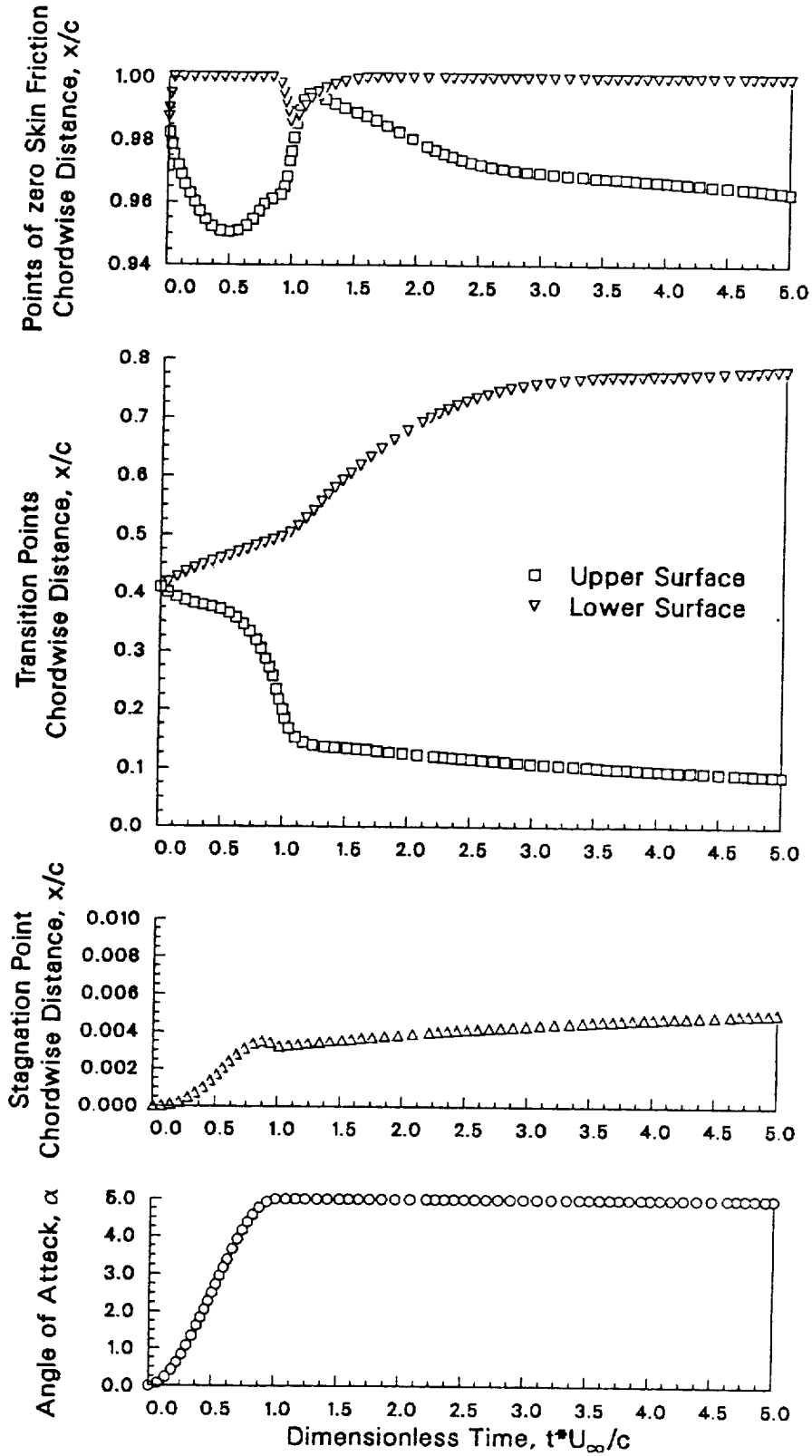


Figure 7. The histories of characteristic points in the flow past a NACA 0012, undergoing a ramp-change in angle of attack.

1. Report No. NASA CR-4198		2. Government Accession No.		3. Recipient's Catalog No.	
4. Title and Subtitle A Numerical Method for Computing Unsteady 2-D Boundary Layer Flows				5. Report Date December 1988	
				6. Performing Organization Code	
7. Author(s) Andreas Krainer				8. Performing Organization Report No. None (E-4394)	
				10. Work Unit No. 582-01-11	
9. Performing Organization Name and Address Naval Postgraduate School Department of Aeronautics Monterey, California 93943				11. Contract or Grant No. C-80017-F	
				13. Type of Report and Period Covered Contractor Report Interim	
12. Sponsoring Agency Name and Address National Aeronautics and Space Administration Lewis Research Center Cleveland, Ohio 44135-3191				14. Sponsoring Agency Code	
15. Supplementary Notes Project Manager, James E. O'Brien, Internal Fluid Mechanics Division, NASA Lewis Research Center.					
16. Abstract A numerical method for calculating unsteady two-dimensional boundary layers in incompressible laminar and turbulent flows is described, and applied to a single airfoil changing its incidence angle in time. The solution procedure adopts a first order panel method with a simple wake model to solve for the inviscid part of the flow, and an implicit finite difference method for the viscous part of the flow. Both procedures integrate in time in a step-by-step fashion, in course of which each step involves the solution of the elliptic Laplace equation and the solution of the parabolic boundary layer equations. The Reynolds shear stress term of the boundary layer equations is modeled by an algebraic eddy viscosity closure, which essentially is the steady Cebeci-Smith model. The location of transition is predicted by an empirical data correlation originating from Michel. Since transition and turbulence modeling are key factors in the prediction of viscous flows, their accuracy will be of dominant influence to the overall results. The presented methodology offers a decisive cost advantage as compared to solvers of the full Navier-Stokes equations. The efficiency of our method derives from its viscous and inviscid components, which both bypass the far more expensive field solution. Conceptually the method makes no assumptions as to the type of motion or the shape of the airfoil, and is subject only to the limitations imposed by the boundary layer approximation and by the assumption of an irrotational inviscid flow field. As a consequence of the currently employed boundary layer approach, in which the pressure is prescribed, the method cannot cope with the problem of flow separation. Future work is planned to address the problem of unsteady flow separation, which will require an interactive coupling of the inviscid and viscous flow solvers.					
17. Key Words (Suggested by Author(s)) Boundary layers			18. Distribution Statement Unclassified - Unlimited Subject Category 34		
19. Security Classif. (of this report) Unclassified		20. Security Classif. (of this page) Unclassified		21. No of pages 64	22. Price* A04

